

7. CURRENT DRIVE

Charles C. Bathke

Robert A. Krakowski

Tak-Kuen Mau

Contents

7.1.	INTRODUCTION	7-1
7.2.	CURRENT-DRIVE OPTIONS	7-2
7.2.1.	Oscillating-Field Current Drive	7-2
7.2.2.	Bootstrap Current	7-5
7.2.3.	Fast-Wave Current Drive	7-6
7.2.4.	Relativistic Electron Beams	7-11
7.3.	OSCILLATING-FIELD CURRENT-DRIVE MODEL	7-12
7.3.1.	Plasma Model	7-12
7.3.2.	Circuit Model	7-22
7.4.	CURRENT-DRIVE PARAMETERS	7-26
7.5.	SUMMARY AND CONCLUSIONS	7-35
	REFERENCES	7-40

7. CURRENT DRIVE

7.1. INTRODUCTION

At full plasma current of 18 MW/m^2 , the energy stored in the reference TITAN plasma includes $W_M \sim 5 \text{ GJ}$ of magnetic energy and 0.1 GJ of kinetic energy. The magnetic stored energies internal to the plasma are 0.3 GJ in the toroidal field and 0.4 GJ in the poloidal field. The magnetic energies outside of the plasma are $< 2 \text{ MJ}$ in the toroidal field and 4 GJ in the poloidal field for zero OH-coils current (6 GJ for OH-coils in full forward-bias current). Since, the toroidal magnetic stored energy internal to the plasma is supplied by the poloidal-field circuit during the start-up, the reference TITAN design requires a poloidal flux of $L_p I_\phi \simeq 250 \text{ Wb}$ to achieve full plasma current. Because of the large plasma resistance in the TITAN designs, an inductively pulsed burn would be sustained for a pulse length of the order of $L_p/R_p \simeq 200$ to 400 s . Therefore, steady-state operation is essential considering issues such as the total power balance, thermal cyclic fatigue in a high-power-density environment, as well as the costs of on-site energy storage (frequent grid-assisted start-up seems unlikely) and thermal storage. An inductively pulsed RFP reactor is a possibility [1]. The parameters of such a reactor, however, should be optimized to minimize the plasma resistance, which results in larger plasmas, lower power density, and possibly the use of superconducting coils throughout the FPC.

A number of current-drive options for the RFP have been considered (Section 7.2). Although the use of radio-frequency (RF) fast-wave current-drive scheme has not been fully explored for the RFP, the high plasma density ($n \sim 9 \times 10^{20} \text{ m}^{-3}$ in TITAN) and currents relative to those for the tokamak indicate problems with the efficiency of RF current-drive schemes. On the other hand, because of the relaxation processes in RFPs, there is no need to drive the current at the plasma center and some of the issues related to wave penetration may be negated. Bootstrap current is also expected to be low, if such current exists at all in RFPs, since β_θ and $\epsilon = r_p/R_T$ are small relative to the tokamak.

The close coupling of poloidal and toroidal currents and magnetic fields that determine the near-minimum-energy states of the RFP offers the possibility of a current-drive method based on “magnetic helicity injection” because the resistive decay of plasma current can be viewed as a dissipation of magnetic helicity [2]. For the TITAN reactors, helicity injection by the oscillating-field current drive (OFCD) has been selected as the means to sustain the toroidal plasma current. From a theoretical viewpoint, the required

physics processes for OFCD in RFPs are identified [3,4], several numerical simulations are summarized in Reference [5], and some experimental data on OFCD [6] are also available (Section 7.2.1). An analogue circuit model for OFCD is presented in Section 7.3 and is used to investigate parametrically the characteristics of the OFCD system for the TITAN reactor. Design points for TITAN-I and TITAN-II are suggested in Section 7.4. Section 7.5 presents a summary and conclusions.

7.2. CURRENT-DRIVE OPTIONS

7.2.1. Oscillating-Field Current Drive

The strong coupling of poloidal and toroidal magnetic fields that determine the near-minimum-energy states of the RFP [7] offers the possibility of a current-drive method based on “magnetic helicity injection” because the resistive decay of plasma current can be viewed as a dissipation of magnetic helicity [2]. Current drive through “electrostatic helicity injection” has been experimentally demonstrated in spheromaks [8], which are also relaxed-state systems like RFPs. Another helicity-injection technique is the oscillating-field current drive (OFCD) [2,9]. In this scheme, audio-frequency oscillating voltages are applied to the toroidal and poloidal circuits in the appropriate phase ($\delta = \pi/2$) to drive a DC toroidal current in the plasma with the plasma, in effect, behaving as a nonlinear rectifier. As originally proposed [2], OFCD is based on the premise that maintenance of the RFP configuration simply requires the supply of magnetic helicity at a rate equal to its dissipation. The helicity balance is given by [2,10]

$$\frac{dK}{dt} = 2\phi V_\phi - 2 \int \mathbf{E} \cdot \mathbf{B} dV_p, \quad (7.2-1)$$

where the integral gives the rate of helicity dissipation throughout the plasma volume and the remaining product of toroidal flux and voltage gives the rate of helicity injection or ejection through the plasma surface. Helicity is effectively injected into the plasma if Φ and V_ϕ are sinusoidal and are oscillated in phase with each other (*e.g.*, $V_\theta = -\dot{\Phi}$ and V_ϕ are in quadrature), even though the time-averaged electric fields are zero. Hence, with the F - Θ diagram providing the required connection between V_θ and V_ϕ , a noninvasive and potentially efficient means to drive currents in high-density thermonuclear plasma is possible. Current drive by helicity injection has also been proposed for tokamaks [11 - 13], provided that a similar, globally nondisruptive mechanism for profile relaxation exists.

Experimental data on OFCD in RFPs are reviewed in detail in Section 2.3.8 [9,6]. Low-power OFCD tests (~ 7 MVA, $I_\phi \simeq 60$ to 70 kA), shown on Figure 7.2-1, were con-

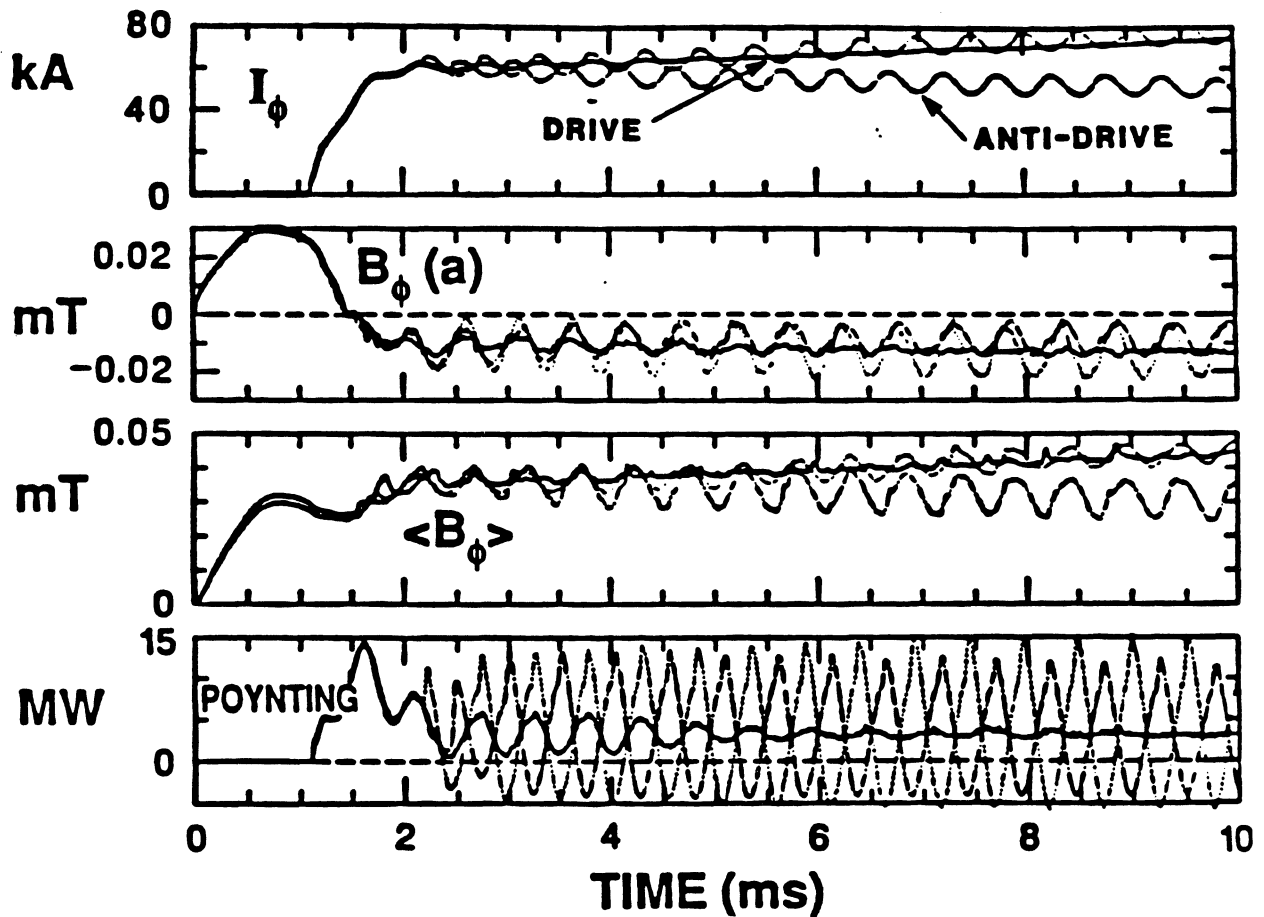


Figure 7.2-1. Low-power OFCD discharge results from Reference [6]. Shown are traces of current, edge toroidal field, toroidal flux, and Poynting vector for a standard discharge, a discharge with the optimal phase between toroidal and poloidal OFCD circuits for driving current, and a discharge with the optimal phase in the OFCD circuit for anti-drive.

ducted on ZT-40M. These ramped discharges were at low temperature and, hence, a high plasma resistance. With optimal phasing ($\delta \simeq \pi/2$), an approximately 5% increase in poloidal flux was observed when OFCD was applied. While a clear demonstration of substantial current drive by OFCD must await RFPs operating with hotter plasmas and reduced wall interaction [14], the strong dependence of the plasma response on δ and the spatial and temporal behavior of the mean magnetic fields are in general agreement with magnetic helicity models and simulations.

Most of the analysis and design for the OFCD system is based on circuit-analogue models [2,9]. Such a model is described in Section 7.3 and is used to analyze the TITAN reactor current-drive system. A heuristic method for explaining OFCD in RFPs on the basis of MHD [5] considers the evolution of the q -profile for one OFCD cycle, as is shown in Figure 7.2-2. Initially the near-minimum-energy RFP state is characterized by a value of $q = d\psi/d\phi$ that is less than unity on axis, with q falling to zero near the plasma edge and reversing at the plasma surface as the toroidal field changes direction. In order to affect OFCD in the RFP, the external toroidal- and poloidal-field circuits are oscillated about steady-state values, with the most efficient “pumping” (*i.e.*, maximum current for minimum reactive power) occurring when the toroidal and poloidal voltages are approximately 90 degrees out of phase. A decrease in the external poloidal flux, ψ , and an increase in amplitude of the external toroidal flux, ϕ , will result in a more negative F value (*i.e.*, deeper reversal) which appears as a compression phase in Figure 7.2-2. The plasma under these conditions is unstable to a series of resistive-MHD modes with high toroidal mode numbers, n , all of which have a poloidal mode number $m = 1$. These instabilities drive a Kadomtsev reconnection process (Figure 7.2-2). resulting in a flattening of the central portion of the q profile and increasing the poloidal flux [3,4]. The Kadomtsev reconnection process may also occur during the compression phase and need not be a distinct phase, as is shown in Figure 7.2-2. The plasma is then decompressed as the external circuits approach the end of a period when the external poloidal flux is increasing and the toroidal flux is decreasing. With the value of q at the plasma edge reset to the initial value, the plasma then relaxes by means of a double reconnection [4] (*i.e.*, dynamo effect) into the initial near-minimum-energy state, and the OFCD cycle is complete. As indicated previously, frequency of a few tens of Hz are generally required for reactor grade plasmas, with higher frequency ($\sim 5,000$ Hz) for the more resistive, present-day experiments.

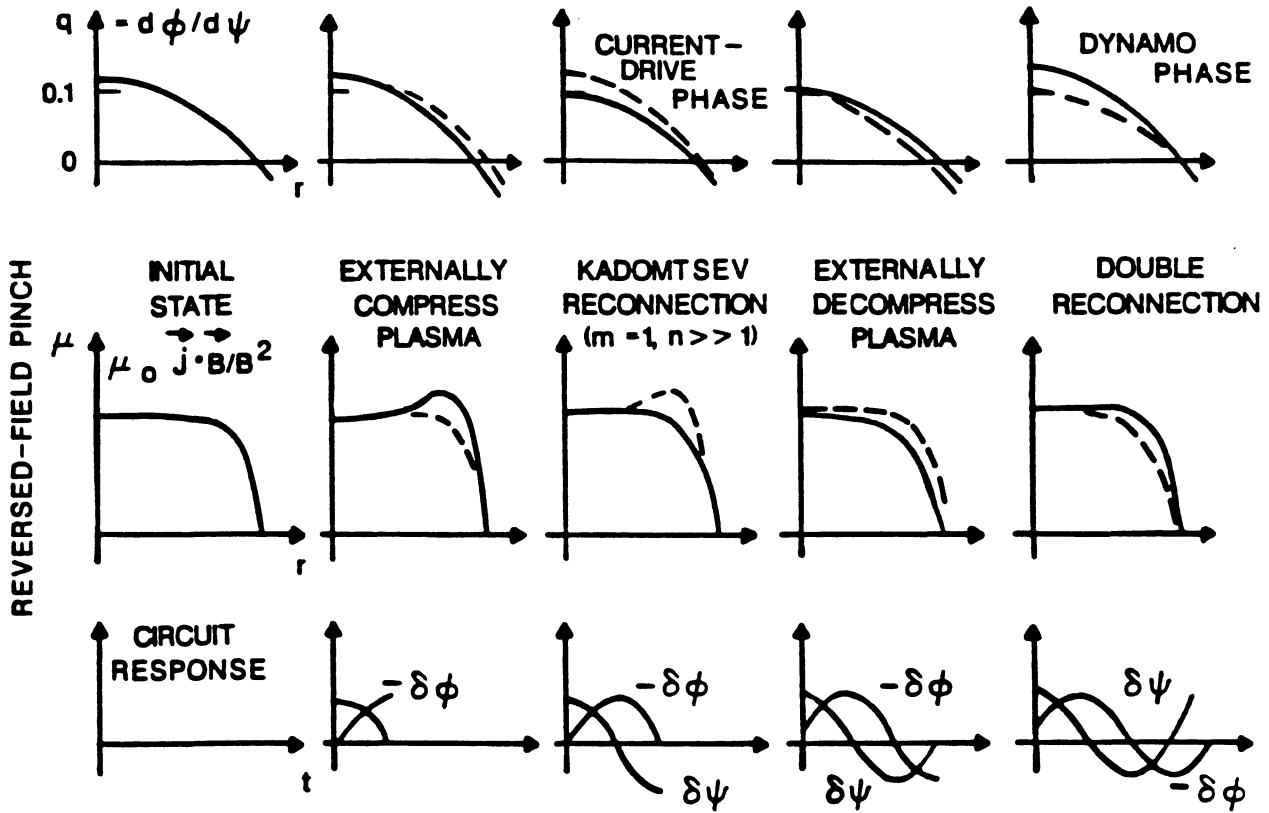


Figure 7.2-2. Schematic representation of OFCD in terms of a q-profile evaluation [5].

7.2.2. Bootstrap Current

Neoclassical theory predicts the existence of a bootstrap current caused by radial diffusion. An expression for this bootstrap current density is given by [15]

$$j_{BC} = -\frac{\epsilon^{1/2}}{B_\theta} \left(\frac{\partial p}{\partial r} \right), \quad (7.2-2)$$

where $\epsilon = r_p/R_T$ is the inverse aspect ratio. The high β_θ that characterizes the RFP suggests a large bootstrap current, but the high aspect ratio will tend to reduce the effect. For example, if the pressure profile is given by $p/p_o = 1 - (r/r_p)^\nu$, then the contribution of bootstrap current to the overall current density is given by

$$\frac{j_{BC}}{j_\phi} = \beta_\theta \epsilon^{1/2} \frac{\nu^2}{4(\nu + 2)}, \quad (7.2-3)$$

which for $\nu \simeq 2$, $\beta_\theta \simeq 0.2$, and $\epsilon \simeq 1/6$ (TITAN conditions) gives $j_{BC}/j_\phi \simeq 0.02$. Significantly steeper pressure gradients and lower aspect ratios would be required to make the

bootstrap current a significant contributor, if it exists at all in RFPs. Bootstrap current is not considered a possibility for TITAN at this time.

7.2.3. Fast-Wave Current Drive

A variety of current-drive methods using radio-frequency (RF) waves have been explored in the context of maintaining a steady-state tokamak reactor [16,17]. These waves are usually classified according to their frequency ranges, namely: electron cyclotron (ECH; ~ 100 GHz), lower-hybrid (LH; ~ 1 GHz), ion cyclotron (ICRF; ~ 100 MHz), and low-frequency Alfvén (AW; ~ 1 MHz). Little experimental and theoretical work has been done for RF current drive in RFPs, particularly as applied to driving poloidal currents in the outer regions of the core plasma.

The most successful RF current-drive experiment to date has been with LH slow waves in a tokamak [18]. In this scheme, the wave energy is launched toroidally in one direction and is absorbed by electrons through the Landau damping process. In essence, the wave electric field accelerates those electrons with parallel speed $v_{\parallel} = \omega/k_{\parallel}$, where ω is the wave frequency and k_{\parallel} is the wave number parallel to the DC magnetic field. These resonant electrons that receive the wave momentum carry a plasma current, which is subsequently dissipated through collisions with the thermal particles. Consequently, accelerating higher energy electrons results in higher current-drive efficiency. For a Maxwellian electron distribution, a higher temperature (T_e) plasma naturally leads to more efficient current drive. Likewise, a denser plasma through collisional dissipation will result in less favorable current-drive efficiency. Disregarding accessibility issues temporarily, the current-drive efficiency, I_{ϕ}/P_{CD} , scales as T_e/n_e . In fact, this conclusion can be extended to other RF schemes, which may drive current by creating a toroidally asymmetric resistivity (*e.g.*, ECH waves) or by minority ion heating (*e.g.*, ICRF waves).

In actuality, many physical processes in the reactor plasma can affect the RF current-drive efficiency: (1) Because of the variation of the magnetic field along the field line, electrons can be trapped in a magnetic well and consequently become incapable of carrying currents. Any portion of the wave power absorbed by these trapped electrons, therefore, will not contribute to the current and will lower the efficiency. (2) Other competing wave damping processes exist that do not result in a current. An example of these damping processes is absorption by the nonthermal alpha particles and fuel ions in the vicinity of their harmonic cyclotron resonance surfaces. Damping by the alpha particles is particularly severe for waves in the LH range of frequencies [19], as will be shown later in this section. (3) In some instances, electron Landau damping may simply be so strong

in the plasma periphery that none of the wave power penetrates to the core where it is most needed. This phenomenon is peculiar to the LH slow wave. (4) The bulk of the wave energy may be deposited in the thermal electrons, which are not efficient current carriers. This suggests that if a high-energy electron component can be created in the plasma, a synergistic effect may occur, in that these relatively collisionless electrons absorb most of the wave energy and carry the resultant current.

The fact that $I_\phi/P_{CD} \propto T_e/n_e$ immediately suggests a rather low efficiency for RF current drive in the core of the TITAN plasma (relatively high density of $9 \times 10^{20} \text{ m}^{-3}$ and moderate temperature of $\sim 10 \text{ keV}$). Moreover, absorption by the large population of alpha particles will also pose a serious accessibility problem for the incoming wave. For instance, the alpha-particle damping length in the TITAN core plasma is of the order of 0.1 m or less for the LH waves. However, in an RFP device, core current drive may not be crucial. The stable field configuration is maintained by the continuous relaxation of the plasma to a force-free, minimum-energy state, in which the current is dominantly toroidal in the plasma center and poloidal in the periphery. It is then plausible to drive a poloidal current in a narrow region just inside the toroidal-field reversal layer ($q = 0$ surface) and allow the inherent turbulent relaxation process to redistribute the induced toroidal flux throughout the entire plasma. As a result, an incremental current is continuously generated to replenish the current lost through ohmic dissipation. The feasibility of this scheme of using waves in the LH range of frequencies in TITAN is examined below.

A 1-D coupled model of RF and plasma should be constructed for the region near the toroidal-field reversal layer, where $|B_\phi| \ll B_\theta$. Neglecting B_ϕ and taking advantage of the approximate poloidal symmetry, therefore, results in a simple, yet sufficient, 1-D radial plasma model. Defining $N_\parallel \approx N_\theta$, and $N_\perp \approx N_r$, where $N = kc/\omega$ is the wave index of refraction, the wave dispersion relation can be written as follows:

$$D(\omega, \mathbf{r}, \mathbf{N}) = P_6 N_\perp^6 + P_4 N_\perp^4 + P_2 N_\perp^2 + P_0 = 0, \quad (7.2-4)$$

where the coefficients P_i are functions of N_\parallel , r , and ω . The electron Landau damping decrement, γ_e , is given by

$$\gamma_e = -\frac{D_I^{(e)}}{\partial D / \partial k_\perp}, \quad (7.2-5)$$

with $D_I^{(e)} = 2\pi^{1/2} (\omega_{pe}/\omega)^2 N_\perp^2 N_\parallel^2 w^3 \exp(-w^2)$ and $w = \omega/(k_\parallel v_e)$. A similar expression exists for electron damping resulting from transit-time magnetic pumping (TTMP), which is more important for the fast wave.

For the important alpha-particle damping decrement, the unmagnetized-ion-orbit model [19] is used because of the large energy of the alpha particles. This model gives the following expression for γ_α :

$$\gamma_\alpha = \frac{\omega (\epsilon_{\parallel} - N_{\perp}^2) \epsilon_{\perp\alpha}}{c \epsilon_{\perp} N_{\perp}}, \quad (7.2-6)$$

for the slow mode, and

$$\gamma_\alpha = \frac{\omega N_{\perp} \epsilon_{\perp\alpha}}{c (N_{\parallel}^2 - \epsilon_{\perp} + \epsilon_{\times}^2 / \epsilon_{\parallel})}, \quad (7.2-7)$$

for the fast mode, where $\epsilon_{\perp\alpha} = 0.2\pi(\omega_{p\alpha}/\omega)^2$ and ϵ_{\perp} , ϵ_{\parallel} , and ϵ_{\times} are the plasma dielectric tensor elements.

The RF power flux, $P(r)$, along the radial direction is then calculated as

$$P(r) = P(r_p) \exp\left(-\int_{r_p}^r \gamma dr'\right), \quad (7.2-8)$$

where $\gamma = \gamma_e + \gamma_\alpha$ and r_p is the plasma radius. To calculate the driven current, the power absorbed by electrons over an incremental radius is determined and averaged over the flux surface to obtain the local absorbed power density, P_e . The local driven current, j_{\parallel}^{rf} , is then given by

$$j_{\parallel}^{rf} = \frac{19.2 \times 10^{18} T_e}{\ln \Lambda} \frac{\hat{\eta}}{n_e} P_e, \quad (7.2-9)$$

with T_e in keV and the other variables in MKS units. In Equation 7.2-9, $\hat{\eta}$ is the Fisch-Karney normalized current-drive efficiency [20] and is given by

$$\hat{\eta} = \frac{8\omega^2}{5+Z} + 2 + \frac{12(6+Z)}{(5+Z)(3+Z)} + \frac{2C}{Z\omega}, \quad (7.2-10)$$

where $Z \equiv Z_{eff}$ and C is 3.76 for Landau damping and 8.09 for TTMP.

Using the nominal TITAN parameters listed in Table 7.2-I and the following density and temperature profiles:

$$n_e(r) = [n_e(0) - n_e(r_p)] [1 - (r/r_p)^{6.25}] + n_e(r_p), \quad (7.2-11)$$

$$T_e(r) = [T_e(0) - T_e(r_p)] [1 - (r/r_p)^{3.4}] + T_e(r_p), \quad (7.2-12)$$

both the fast and slow waves have been examined as a means to drive current in the plasma periphery. For the slow mode, severe accessibility problems exist at the plasma

Table 7.2-I.

PARAMETERS FOR TITAN RF CURRENT-DRIVE ANALYSIS

Plasma current, I_ϕ (MA)	17.82
Major plasma radius, R_T (m)	3.6
Minor plasma radius, r_p (m)	0.6
Reversal surface minor radius, r_r (m)	0.55
Poloidal field at radius r , $B_\theta(r)$, (T)	$17.3 J_o(5.17r)$
Average electron density, n_e (m^{-3})	8.9×10^{20}
Edge electron density, $n_e(r_p)$ (m^{-3})	1.6×10^{20}
Density peaking ratio, $n_e(0)/n_e$	1.26
Average electron temperature, T_e (keV)	9.6
Edge electron temperature, $T_e(r_p)$ (keV)	0.25
Temperature peaking ratio, $T_e(0)/T_e$	1.57
Average electron temperature, T_e	9.6

edge because of the high density. Mode conversion to the fast wave or to the ion plasma wave is dominant, with the latter process leading to undesirably strong fuel ion and alpha-particle damping. For the fast wave in the LH regime, coupling to the slow mode also presents a severe problem, resulting in the wave energy being trapped in the plasma edge. This problem, however, can be overcome by lowering the frequency to achieve complete decoupling from the slow wave.

Results at a frequency of $\omega = 1$ GHz are given in Figure 7.2-3, with $N_{\parallel} = 1.2, 1.5, 2.0, 2.5,$ and 3.0 . It is clear that the wave power damps over a very short radial distance (≤ 0.15 m) inside the separatrix, as is shown in Figure 7.2-3(A). Also, the lower the value of N_{\parallel} , the weaker the absorption and the deeper the penetration. For the purpose of driving poloidal currents inside the $r = 0.48$ -m surface, only the $N_{\parallel} = 1.2$ and 1.5 wave spectral components are desirable. As seen in Figure 7.2-3(B), the generated current profiles for these two components are relatively broad and low compared with those of

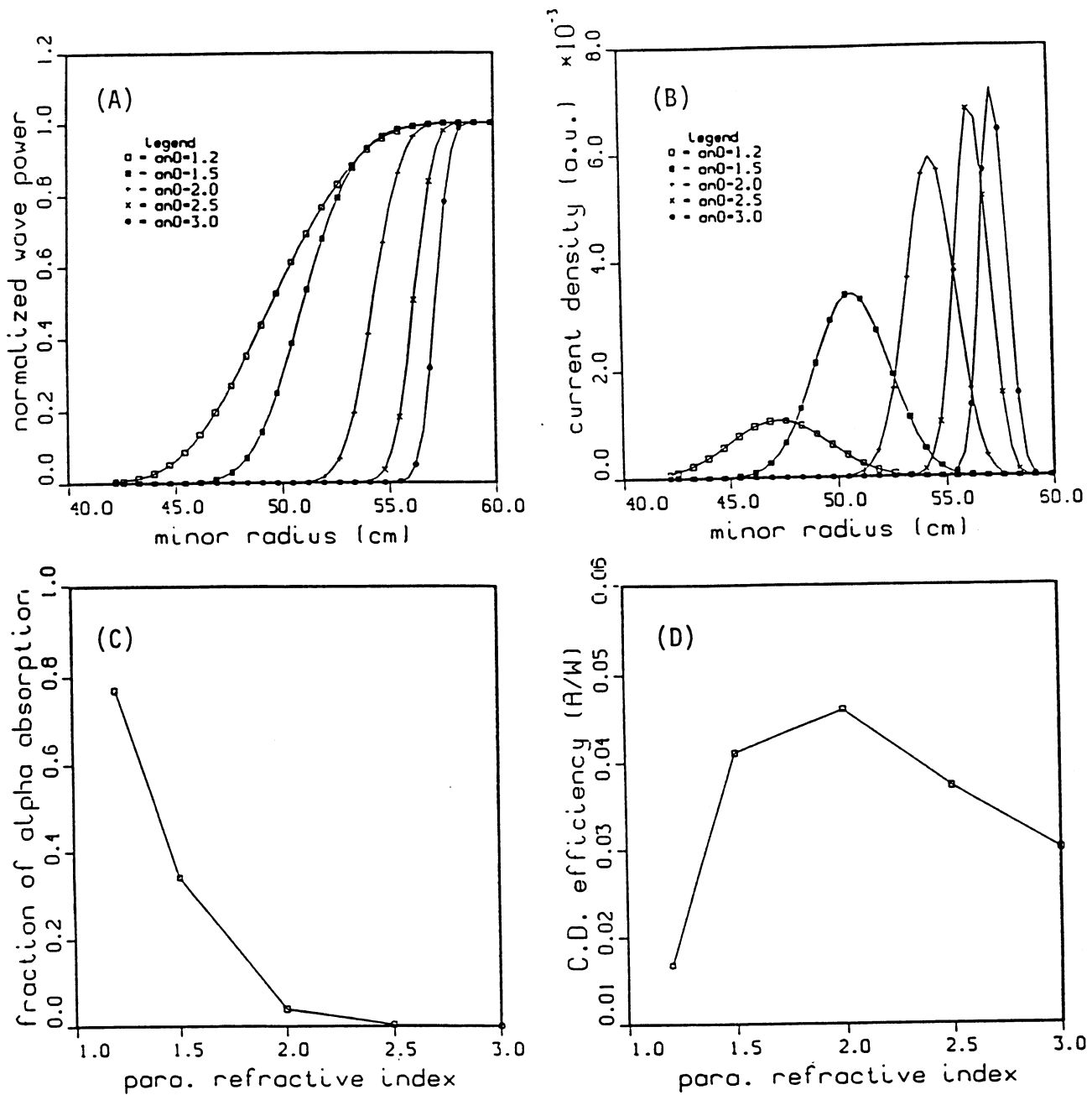


Figure 7.2-3. Profiles of the normalized wave power (A) and RF-driven current-density (B) along the plasma minor radius for a LH fast wave launched into TITAN, with $\omega = 1$ GHz and $N_{\parallel} = 1.2, 1.5, 2.0, 2.5$ and 3.0 , respectively. Also shown are fraction of power absorbed by alpha particles (C) and the resultant current-drive efficiency (D) as functions of N_{\parallel} .

the high- N_{\parallel} components. In Figure 7.2-3(C), it is found that a large portion of the wave energy is deposited in the alpha particles for the low- N_{\parallel} modes; likewise their current-drive efficiencies are low (< 0.05 A/W). The means by which this edge current-drive efficiency will translate into an overall efficiency when the turbulent relaxation process is taken into account, however, is not clear. An assessment of this efficiency requires solving the radial flux-diffusion equation in the presence of a localized toroidal-flux generator inside the $q = 0$ surface which is not within the scope of this work. Given the low current-drive efficiency, even at the plasma periphery, it is unlikely that the global efficiency will be found to be within the range desired.

Basically, the low current-drive efficiency found for the LH fast waves results from the high density and modest temperature found in the periphery of the TITAN plasma. This current-drive scheme relies on the external RF power to distort the electron velocity distribution asymmetrically along the direction of the DC magnetic field. Collisional scattering of the distorted velocity space with the background plasma tends to rapidly restore the distribution to a Maxwellian. In a high-density and low-temperature plasma, this restoring force becomes strong and substantial wave energy is required to maintain the non-Maxwellian distribution under these conditions. In fact, as mentioned earlier, all the conventional RF current-drive schemes use the same mechanism, whether it is ECH, ICRF, LH, or AW, and are not expected to yield a good current-drive efficiency under TITAN plasma conditions. Using synergistic effects by creating a high-energy component in the plasma *a priori* and having the incoming wave damped on these electrons may improve somewhat the resultant current-drive efficiency. This particular method, however, has not been examined in this study.

7.2.4. Relativistic Electron Beams

Reference [21] presents a detailed analysis and design for a relativistic electron-beam (REB) current-drive system for the FED-A fusion device. Those calculations indicate that the current-drive power for such a system can be taken approximately as

$$P_{REB} = 2I_{\phi}^2 R_p, \quad (7.2-13)$$

where R_p is the plasma resistance. Applying Equation 7.2-13 to the TITAN reactor with $I_{\phi} \simeq 18$ MA results in a current-drive system with 16 MW of REB power, consistent with a 1.6-MJ pulse energy and a period of 0.1 s between pulses. The REB current drive has been demonstrated experimentally on several tokamaks and has been used successfully for start-up without the use of OH coils.

Although the low-power requirement makes REBs attractive, a number of obstacles to implementation can be identified: (1) The REB current-drive system involves the repeated firing of megavolt capacitor banks, giving rise to questions of reliability when applied to a commercial reactor. (2) Theory indicates that the REB current will only penetrate a few centimeters into the plasma, leading to a hollow current profile. Deeper penetrations can be achieved if very high voltages (~ 50 MV) are used. One hope in dealing with the hollow current profile is that the REB-created currents will diffuse rapidly into the plasma core through anomalous processes or be transported into the central plasma through MHD activities. A quantitative assessment of these ideas must await future studies.

7.3. OSCILLATING-FIELD CURRENT-DRIVE MODEL

This section develops a methodology [10] by which a power-flow analysis of OFCD, illustrated schematically in Figure 7.3-1, can proceed based on energy balance rather than helicity balance. In developing and evaluating a global picture of OFCD, the circuit parameters and definitions summarized in Table 7.3-I are used to arrive at the OFCD plasma equation which is then incorporated into an overall circuit model and used to obtain the parametric OFCD results reported in Section 7.4.

7.3.1. Plasma Model

The plasma is described in terms of the plasma magnetic helicity, K , toroidal flux, ϕ , and magnetic energy, W_M . The relationship between these parameters and the circuit variables (*i.e.*, resistances, inductances, currents, voltages) constitutes the overall current-drive model. The time dependence of K , ϕ , and W_M results directly from the Maxwell equations:

$$\frac{dK}{dt} = 2\phi V_\phi - 2 \int \eta \mathbf{j} \cdot \mathbf{B} dV_p, \quad (7.3-1)$$

$$\frac{d\phi}{dt} = V_\theta, \quad (7.3-2)$$

$$\frac{dW_M}{dt} = I_\phi V_\phi - I_\theta V_\theta - \int \eta \mathbf{j} \cdot \mathbf{j} dV_p, \quad (7.3-3)$$

$$E_\phi = \eta j_\phi - \alpha B_\phi, \quad (7.3-4)$$

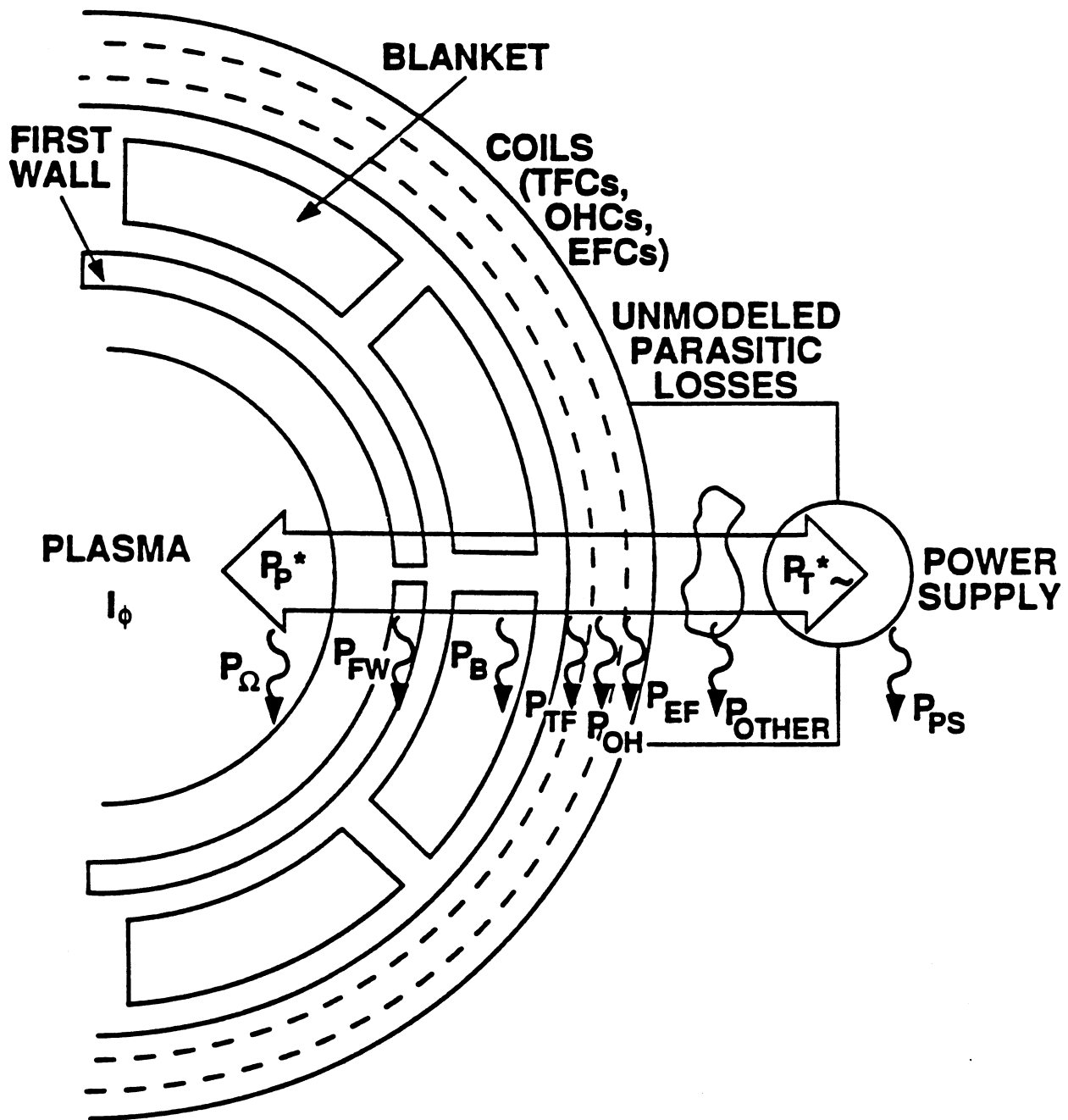


Figure 7.3-1. A simple power-flow diagram for the OFCD model. Shown are the plasma with a dissipation of P_Ω , first wall (P_{FW}), blanket (P_B), toroidal-field coils (P_{TF}), ohmic-heating coils (P_{OH}), equilibrium-field coils (P_{EF}), and power supply (P_{PS}).

Table 7.3-I.
OFCD MODEL DEFINITIONS AND NOTATION

Toroidal voltage on plasma	V_ϕ
Toroidal current in plasma	I_ϕ
Poloidal voltage at plasma surface	$V_\theta = \partial\phi / \partial t \equiv \dot{\phi}$
Poloidal current in external conductors	I_θ
Plasma resistance	R_p
Magnetic helicity	$K = (1/\mu_o) \int \mathbf{A} \cdot \mathbf{B} dV_p$
Toroidal flux	$\phi = 2\pi \int_0^{r_p} B_\phi(r) r dr$
Total field energy within plasma	$W_M = \int_0^{r_p} (B^2/2\mu_o) dr$
Vacuum toroidal inductance	$L_o = \mu_o r_p^2 / 2R_T$
Inverse aspect ratio	$\epsilon = r_p / R_T$
Average toroidal field within plasma	$\langle B_\phi \rangle = \phi / \pi r_p^2$
Reversal parameter	$F = B_\phi(r_w) / \langle B_\phi \rangle = L_o I_\theta / \phi$
Pinch parameter	$\Theta = B_\theta(r_w) / \langle B_\phi \rangle = L_o I_\phi / \epsilon \phi$

where a positive Faraday's-law convention is adopted for the toroidal circuit to orient ϕ and I_ϕ in the same direction and the last expression is the toroidal component of the Ohm's law, $\mathbf{E} = \eta \mathbf{j} - \mathbf{v} \times \mathbf{B}$, corrected for the plasma dynamo effect.

With the plasma resistance defined in terms of a classical resistivity, η [22,23], according to

$$I_\phi^2 R_p = \int \eta \mathbf{j} \cdot \mathbf{j} dV_p, \quad (7.3-5)$$

the plasma helicity and energy equations become

$$\frac{dK}{dt} = 2\phi (V_\phi - I_\phi R_H), \quad (7.3-6)$$

$$\frac{dW_M}{dt} = I_\phi V_\phi - I_\theta V_\theta - I_\phi^2 R_p, \quad (7.3-7)$$

where the helicity dissipation term of Equation 7.3-1 is written in terms of a “helicity resistance,” R_H , defined by $2\phi I_\phi R_H \equiv 2 \int \eta \mathbf{j} \cdot \mathbf{B} d\tau$. For the special case of $\beta = 0$ with a constant μ profile (Bessel-function model, BFM), the helicity resistance is exactly equal to the plasma resistance [22]. Denoting time-averaged quantities by $\langle \rangle$, Equation 7.3-6 shows that for $\langle dK/dt \rangle$ to be equal to zero, then $2\langle \phi V_\phi \rangle$ must equal the dissipation term, which in turn implies that ϕ and V_ϕ should be nominally in phase. Hence, $V_\theta = d\phi/dt$ and V_ϕ should be out of phase by 90° for an optimal OFCD effect.

The plasma magnetic energy, W_M , can be written in terms of plasma and circuit parameters as follows:

$$W_M = \frac{1}{2} L_p I_\phi^2 + \frac{\phi^2}{2L_o}, \quad (7.3-8)$$

where L_p is a plasma internal inductance that does not include vacuum toroidal flux and L_o is the vacuum toroidal inductance defined in Table 7.3-I. Combining Equations 7.3-2, 7.3-7, and 7.3-8 leads to the following expression for the toroidal voltage around the plasma, V_ϕ :

$$V_\phi = I_\phi R_p + \left(L_p + \frac{\Theta}{2} \frac{dL_p}{d\Theta} \right) \dot{I}_\phi + \left(\frac{1-F}{\epsilon\Theta} - \frac{\epsilon\Theta^2}{2L_o} \frac{dL_p}{d\Theta} \right) V_\theta, \quad (7.3-9)$$

where $V_{\phi,\theta}$ are the toroidal and poloidal voltages applied to the plasma. If (1) the coupling of fields is sufficiently strong to make L_p a function of Θ , and (2) if a mechanism exists to allow the perturbation to the near-minimum-energy state to be relaxed to some point in F - Θ space on a time scale of relaxation, τ_R , then oscillations of $V_{\phi,\theta}$ in proper phase at frequency less than $\sim 2\pi/\tau_R$ can give a net time-averaged current, $\langle I_\phi \rangle$, with $\langle V_\phi \rangle = 0$ (*i.e.*, no net flux change). Hence, a nonintrusive means to drive current using primarily the main confining coil system in a low-frequency, low-amplitude plasma-oscillation mode becomes possible.

In evaluating Equation 7.3-9 to determine the flux changes, field oscillations, and power flows, the relationship between F and Θ , as well as the dependence of field and current profiles on Θ in order to determine L_p and R_p , must be determined. A 1-D MHD model described in Section 5 is used for these calculations. The MHD model is based on the following specification of the current density parallel and perpendicular to the magnetic field:

$$\mathbf{j}_\parallel = \mu \mathbf{B}, \quad (7.3-10)$$

$$\mathbf{j}_\perp = \frac{\nabla p \times \mathbf{B}}{B^2}, \quad (7.3-11)$$

$$\nabla \times \mathbf{B} = \mu_o \mathbf{j} = \mu_o (\mathbf{j}_\parallel + \mathbf{j}_\perp), \quad (7.3-12)$$

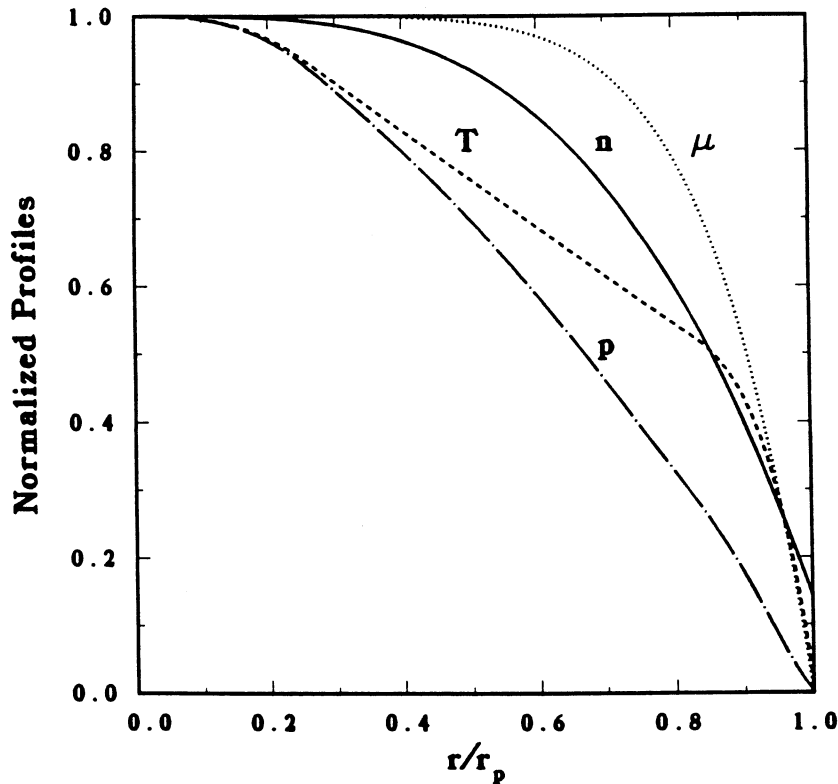


Figure 7.3-2. Normalized density, temperature, and μ profiles from Section 5.3 which are used in the 1-D MHD model.

where μ_o is the permeability of free space. The first equation invokes the Taylor minimum-energy state [7], the second equation gives the prescription for supporting a plasma pressure, p , in equilibrium, and the last equation is Ampere's law. The MHD model requires μ and pressure profiles as input. The pressure profile is derived from an assumed μ profile and from fits to density and temperature profiles calculated with the 1-D plasma simulations (Section 5.3) and shown in Figure 7.3-2.

Equations 7.3-10 through 7.3-12 are solved for field and current-density profiles by specifying Θ subject to the following constraints of fixed β_θ and I_ϕ :

$$\beta_\theta = \frac{4\mu_o}{r_p^2 B_\theta^2(r_p)} \int_0^{r_p} p r dr, \quad (7.3-13)$$

$$I_\phi = 2\pi \int_0^{r_p} j_\phi r dr. \quad (7.3-14)$$

Plasma magnetic-field and current-density profiles corresponding to the mean steady-state plasma conditions for TITAN (*i.e.*, $\langle \Theta \rangle = 1.556$, $\langle \beta_\theta \rangle = 0.22$, and $\langle I_\phi \rangle = 17.82$ MA)

are shown in Figure 7.3-3. Since the pressure profile (derived from the density and temperature profiles of Figure 7.3-2) has a non-zero first derivative at the plasma edge, the plasma has a surface current (*i.e.*, a non-zero current density at the plasma edge) as is shown in Figure 7.3-3; this condition is inconsistent with a toroidal-field null. The surface currents are small, however, and should produce a negligible effect on the results based on this model.

The F - Θ curve shown in Figure 7.3-4 is generated by the repeated application of the 1-D MHD model over a range of Θ values. To generate the F - Θ curve, the plasma current is assumed to scale linearly with Θ . In order to obtain a finite current density at $\Theta \sim 0$ and a finite plasma resistance as predicted in the BFM [22], a $\beta_\theta(\Theta) \propto \Theta^2$ scaling must be used. This β_θ scaling gives rise to an inconsistency with the use of divertors. The plasma separatrix in TITAN is held stationary during OFCD to avoid periodically forcing the plasma into the first wall. This stationary plasma condition is achieved by oscillating the divertor coils in synchronization with the toroidal-field (TF) coils and should result in a plasma pressure invariant to changes in Θ . The effect of using a pressure invariant scaling (*i.e.*, $\beta_\theta(\Theta) \propto \Theta^{-2}$) produces only a 1% change in the current-drive efficiency reported in Section 7.4 compared to values for $\beta_\theta(\Theta) \propto \Theta^2$ scaling. The plasma inductance and resistance are also calculated as functions of Θ and shown in Figure 7.3-5. These results are based on the plasma magnetic-field and current-density profiles obtained with the $\beta_\theta(\Theta) \propto \Theta^2$ scaling.

The poloidal- and toroidal-circuit equations, coupled through Equation 7.3-9, can be solved numerically for I_ϕ once driver functions, such as those given below, are selected for ϕ and V_ϕ :

$$\phi = \phi_o + \delta\phi \cos \omega t , \quad (7.3-15)$$

$$V_\theta = \dot{\phi} = \delta\phi\omega \sin \omega t , \quad (7.3-16)$$

$$V_\phi = \delta V_\phi \cos \omega t . \quad (7.3-17)$$

The computational algorithm for solving Equation 7.3-9 is shown in Figure 7.3-6. This algorithm fixes the value of $\delta\phi/\phi_o$ and iterates on the value of $\delta V_\phi/V_{\phi o}$ until the plasma-current solution to Equation 7.3-9 becomes periodic, *i.e.*, $I_\phi(t) = I_\phi(t + 2\pi/\omega)$. The plasma current is reset to the desired value at the beginning of each simulation period. In an outer loop the time scale is adjusted to ensure that the mean current during a period is the same as the current at the beginning of the period. Another loop that is not operated at present adjusts the μ and pressure profiles to achieve a value of R_H which conserves helicity.

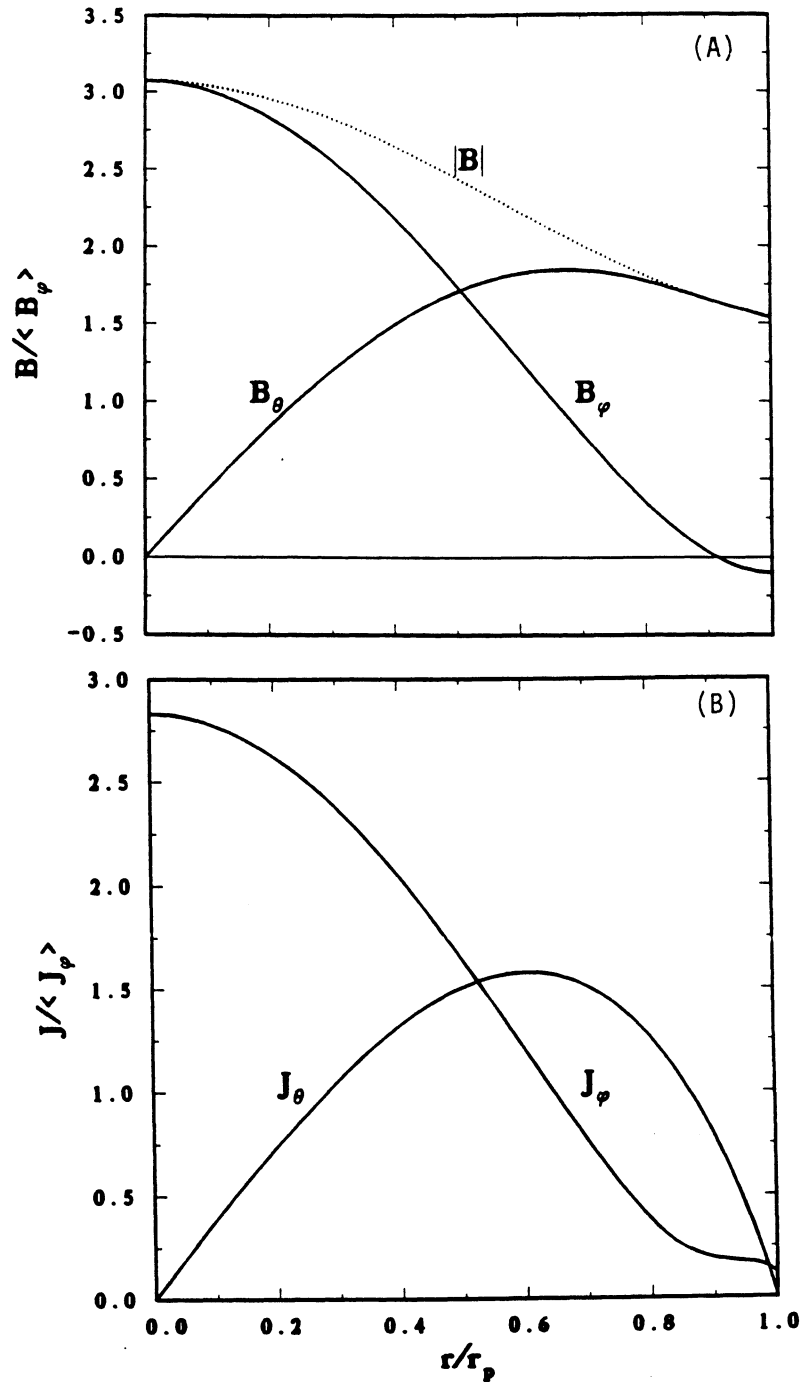


Figure 7.3-3. The profiles of the plasma magnetic field (A) and current density (B) calculated by the 1-D MHD model and used to determine the magnetic energy and plasma inductance for $\beta_\theta = 0.22$ (includes energetic alpha-particle pressure) and $I_\phi = 17.82$ MA.

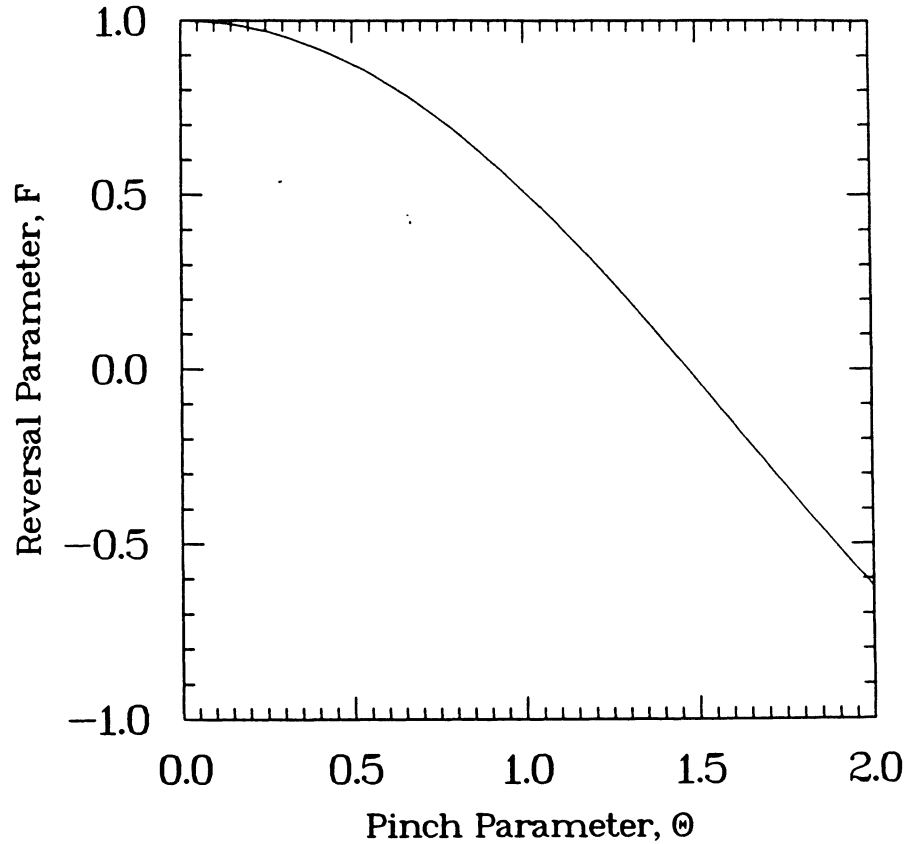


Figure 7.3-4. The F - Θ curve produced by the 1-D MHD model for the OFCD calculations.

The algorithm described in Figure 7.3-6 requires an initial guess for δV_ϕ . The constraint that the time-averaged helicity is constant, $\langle dK/dt \rangle = 0$, can be used to estimate the magnitude of the field oscillations required to sustain a given toroidal plasma current. If the ohmic dissipations for both the induced and driven cases are similar, and if the induced case is characterized by ϕ_o and $V_{\phi o}$, then dK/dt for the driven case is given by Equation 7.3-6 with $V_{\phi o} \equiv I_\phi R_H \simeq I_\phi R_p$. Hence,

$$\frac{dK}{dt} \simeq 2\phi(V_\phi - V_{\phi o}). \quad (7.3-18)$$

Using the driver functions given by Equations 7.3-15 through 7.3-17, the time average of dK/dt for the driver case given above becomes

$$-\left\langle \frac{dK}{dt} \right\rangle = \delta\phi\delta V_\phi + 2\phi_o V_{\phi o}. \quad (7.3-19)$$

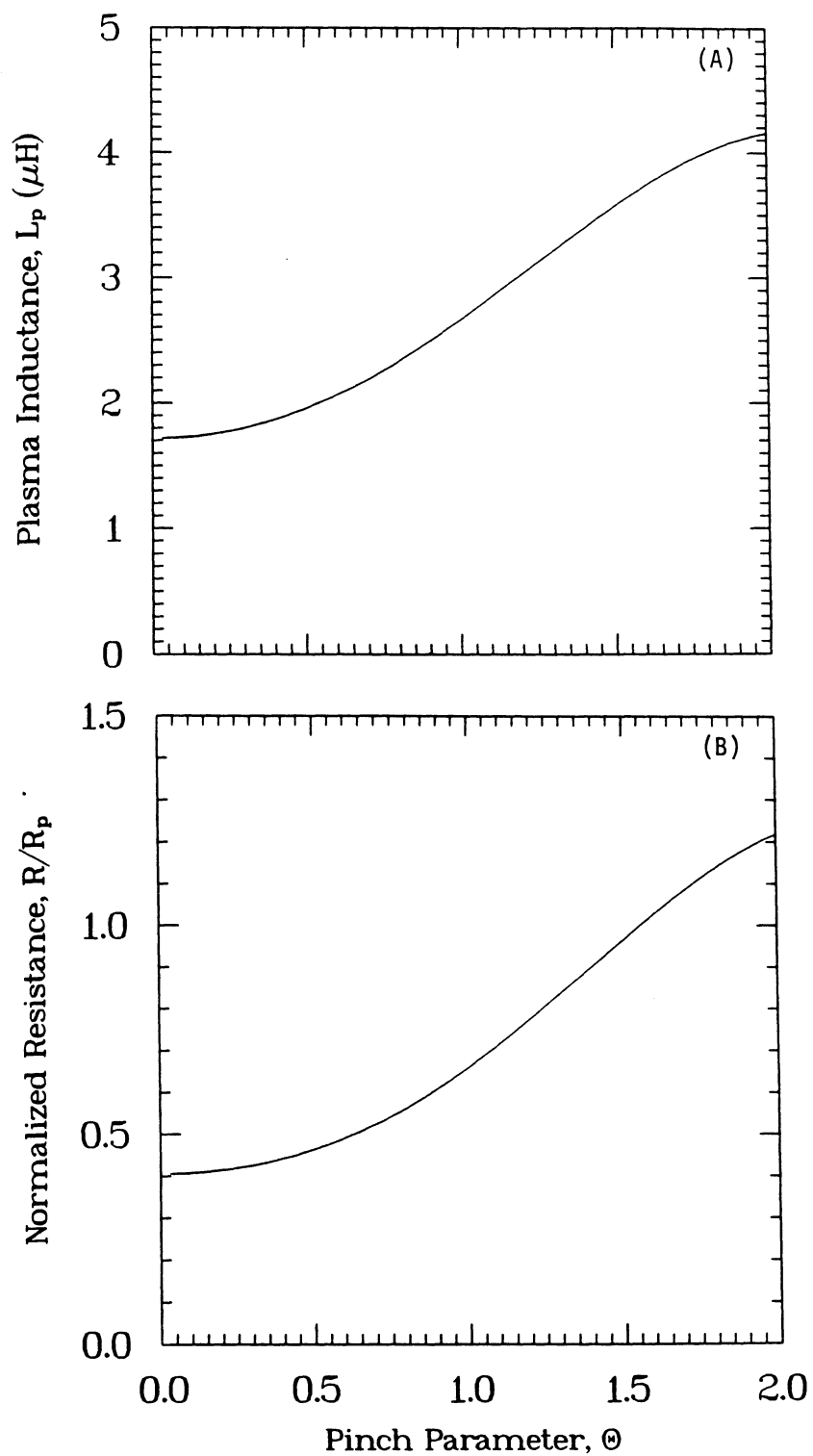


Figure 7.3-5. The dependence of the plasma inductance (A) and resistance (B) on Θ as determined by the 1-D MHD model.

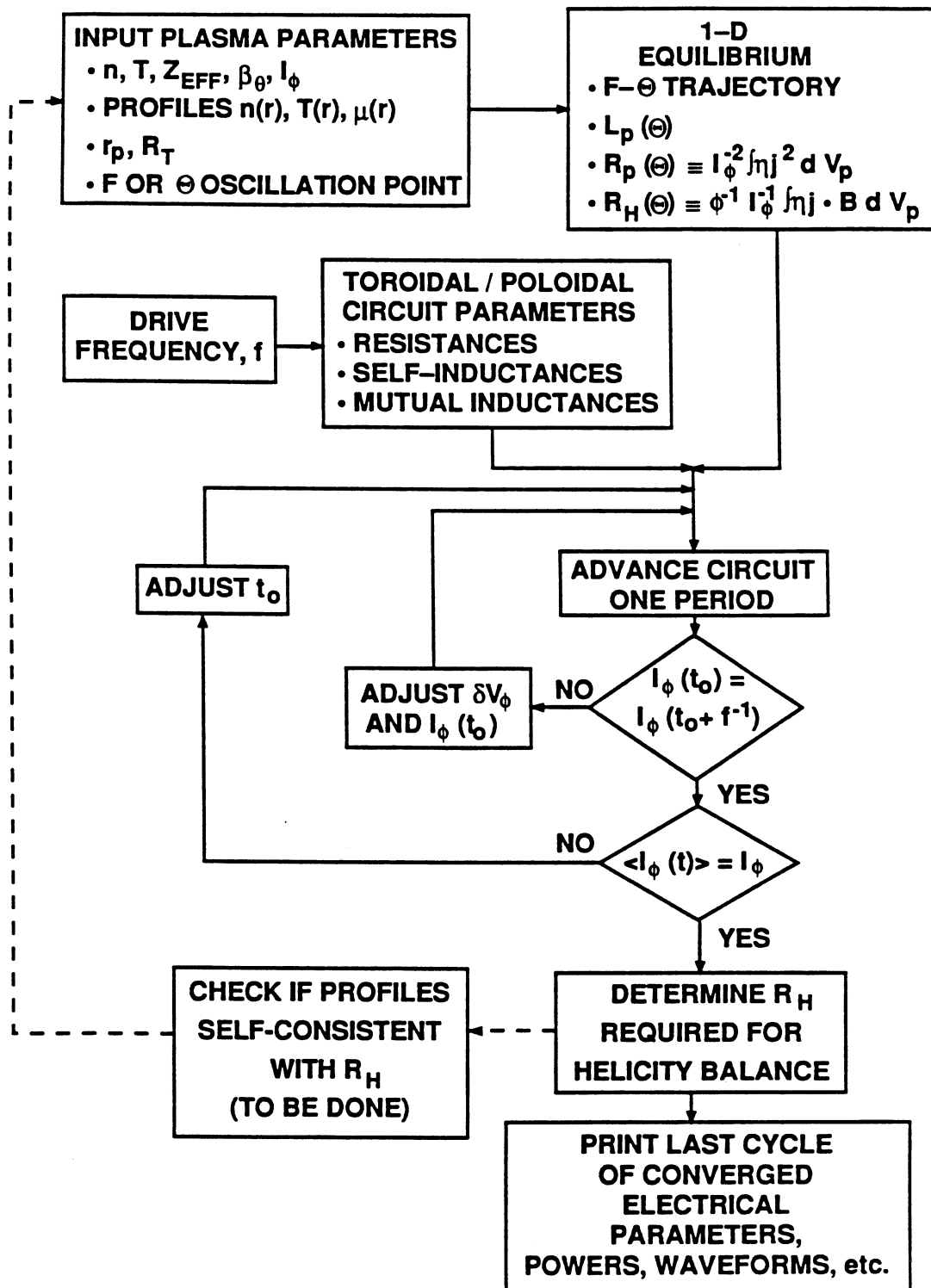


Figure 7.3-6. The algorithm used to solve OFCD plasma/circuit equations.

For $\langle dK/dt \rangle \simeq 0$, the following condition on the amplitudes of the toroidal flux and voltage oscillation results:

$$\left(\frac{\delta\phi}{\phi_o} \right) \left(\frac{\delta V_\phi}{V_{\phi o}} \right) \simeq -2. \quad (7.3-20)$$

Because toroidal-flux oscillations much above $\delta\phi/\phi_o \simeq 0.05$ are expected to seriously impact the RFP configuration (*i.e.*, loss of toroidal-field reversal), the AC toroidal voltage needed to drive a DC toroidal current with $\langle dK/dt \rangle \simeq 0$ can be ~ 40 times greater than the voltage needed to sustain an inductively driven RFP.

7.3.2. Circuit Model

An assessment of OFCD efficiency requires the modeling of the circuit elements external to the plasma in addition to the plasma itself, as indicated schematically in Figure 7.3-1. The governing matrix circuit equation is written as follows:

$$\underline{\underline{\mathbf{L}}} \frac{d}{dt} \underline{\mathbf{I}} + \underline{\underline{\mathbf{R}}} \underline{\mathbf{I}} = \underline{\mathbf{V}}, \quad (7.3-21)$$

where $\underline{\mathbf{I}}$ and $\underline{\mathbf{V}}$ are column vectors representing the currents and voltages, respectively, $\underline{\underline{\mathbf{R}}}$ is a diagonal matrix of resistances, $\underline{\underline{\mathbf{L}}}$ is the inductance matrix, and the inductances are assumed invariant in time. Separate matrix circuit equations are derived for poloidal, θ , and toroidal, ϕ , current paths and are labeled according to the current direction, θ and ϕ , respectively.

A shell model is used to determine the inductances and the resistances used in the respective matrices. The self-inductances in the toroidal and poloidal direction for the i th element are given, respectively, by

$$L_{i,\phi} = \mu_o R_T \left[\ln \left(\frac{R_T}{r_c} \right) - 2 \right], \quad (7.3-22)$$

$$\begin{aligned} L_{i,\theta} = \mu_o R_T & \left[1 - (1 - \gamma_I^2)^{1/2} - \frac{1}{3} (1 - \gamma_O^2)^{1/2} (2 + \gamma_O^2) \right. \\ & + \gamma_O (\gamma_O - \gamma_I)^{-2} (\sin^{-1} \gamma_I - \sin^{-1} \gamma_O) \\ & \left. + \frac{1}{3} (\gamma_O - \gamma_I)^{-2} (1 - \gamma_I^2)^{1/2} (2 + \gamma_I^2 + 3\gamma_O^2 - 3\gamma_O \gamma_I) \right], \quad (7.3-23) \end{aligned}$$

where $\gamma_I = r_I/R_T$ and $\gamma_O = r_O/R_T$, the major and minor radii of the shell are R_T and r_c , and the inner and outer minor radii of the shell are r_I and r_O , respectively. The

internal inductance is ignored in Equation 7.3-22. The mutual inductance between the i th and j th elements, M_{ij} , is the smaller of the i th and j th self-inductances in the shell model. The mutual inductance between two elements then is the self-inductance of the element with the smaller minor radius for poloidal currents and that of the element with the larger minor radius for toroidal currents. The resistance of the i th element is

$$R_i = \frac{2\eta_i R_T}{r_O^2 - r_I^2}, \quad (7.3-24)$$

where η_i is the resistivity of the material in the conducting shell. The circuit elements simulated are the plasma, first wall (FW), the toroidal-field (TF) coils, a portion of the windings of the ohmic-heating (OH) coils, a primary equilibrium-field (EF) coil set, a secondary EF-trim coil set, and the reflector and shield (R/S) for the TITAN-I and the blanket for the TITAN-II,

The current vector $\underline{\mathbf{I}}$ in Equation 7.3-21 has components corresponding to each circuit element. The plasma current in the toroidal-circuit version of Equation 7.3-21 is the I_ϕ solution to Equation 7.3-9. The plasma current in the poloidal-circuit version of Equation 7.3-21 is a model artifact required for inductive transfer of magnetic-field energy to the plasma from the external elements and resembles a plasma skin current (physically, it is not a skin current).

The self-inductances and resistances used for constructing $\underline{\mathbf{L}}$ and $\underline{\mathbf{R}}$ matrixes in Equation 7.3-21 are presented in Table 7.3-II and Table 7.3-III, respectively, for TITAN-I and TITAN-II. The TF-coil set for TITAN-I has been separated into six individual elements that physically correspond to the six radial rows of integrated-blanket-coil (IBC) tubes (Section 4.3.2). This configuration is used because the tube rows are connected electrically in parallel (Section 10.5) and the current penetration skin depth at the frequencies considered (~ 25 Hz) is comparable to the tube diameter. The plasma resistance is taken as zero in Equation 7.3-21, because the plasma resistance is included in Equations 7.3-7 and 7.3-9. The plasma inductances listed in Tables 7.3-II and 7.3-III are only the external inductances; the internal inductances appear in Equations 7.3-8 and 7.3-9.

The voltage vector, $\underline{\mathbf{V}}$, in Equation 7.3-21 contains time-varying applied voltages for the elements in which current is driven (*i.e.*, the TF, OH, EF, and trim coil sets). The voltage on the TF coil is determined by requiring the toroidal field at the plasma surface be produced by all the elements with continuous poloidal current paths. The voltage of the OH coil is derived from knowing the solution for I_ϕ from Equation 7.3-9. In the case of the EF coil, the voltage is maintained at a constant value corresponding

to the mean equilibrium field. The EF trim-coil voltage is determined by requiring the trim coil to track the oscillating equilibrium-field requirement of the plasma [4]. For the passive elements, FW and R/S, the voltages are zero. The plasma voltage in the toroidal-circuit version of Equation 7.3-21 is taken to be $-V_\phi$, because V_ϕ is a voltage drop in Equation 7.3-9. In the poloidal-circuit equation, the plasma voltage is taken to be V_θ , because of the decision to use a positive Faraday's law (Equation 7.3-2).

Table 7.3-II.

CIRCUIT PARAMETERS FOR TITAN-I OFCD ANALYSIS

Circuit Element	Inductance (μH)		Resistance ($\mu\Omega$)	
	Toroidal	Poloidal	Toroidal	Poloidal
Plasma	9.56	0.0580	0.	0.
First wall:				
without gaps	9.06	0.07	760.	6.95
with gaps	0.0387	0.00114	3,040.	27.8
TF coil:				
1st tube row	—	0.0786	—	2.83
2nd tube row	—	0.0896	—	2.96
3rd tube row	—	0.101	—	3.09
4th tube row	—	0.114	—	3.22
5th tube row	—	0.127	—	3.35
6th tube row	—	0.141	—	3.48
OH coil	5.15	—	1.51	—
Reflector & shield	1.65	0.161	25.2	2.33
EF coil	0.752	—	$\sim 0.$	—
Trim coil	3.18	—	2.93	—

Table 7.3-III.
CIRCUIT PARAMETERS FOR TITAN-II OFCD ANALYSIS

Circuit Element	Inductance (μH)		Resistance ($\mu\Omega$)	
	Toroidal	Poloidal	Toroidal	Poloidal
Plasma	9.56	0.0580	0.	0.
First wall	0.0387	0.00114	3,040.	27.8
TF coil	–	0.225	–	0.525
OH coil	5.15	–	1.51	–
Blanket	2.60	0.144	642,000.	33,000.
EF coil	0.752	–	$\sim 0.$	–
Trim coil	3.18	–	2.93	–

Calculations with a continuous first wall (Section 7.4) indicate a need to model passive elements with resistive breaks or gaps. The model derived here treats each passive element as consisting of an inner and outer current path, as is shown in Figure 7.3-7. The current is assumed to flow in the smaller of (1) half of the radial build of the passive element or (2) a current penetration skin depth. The self-inductance of the element with gaps is the difference of the self-inductances of the inner and outer current-path elements. The mutual inductance between an element with gaps and a continuous element is the difference of the minimum of the self-inductances of the inner current-path element and the continuous element and the minimum of the self-inductances of the outer current-path element and the continuous path element. If the continuous element has a smaller self-inductance than either the inner or outer current-path elements, then a zero mutual inductance results in the shell model. The resistance of the element with gaps is the sum of the resistances of the inner and outer current-path elements. This eddy-current model yields an accurate accounting of dissipated power when the oscillating magnetic fields are tangential to the passive elements, as is shown in Section 4.6.2.

The time-dependent current and voltage solutions to the toroidal and poloidal versions of Equation 7.3-21 are solved in conjunction with the $I_\phi(t)$ solution to Equation 7.3-9.

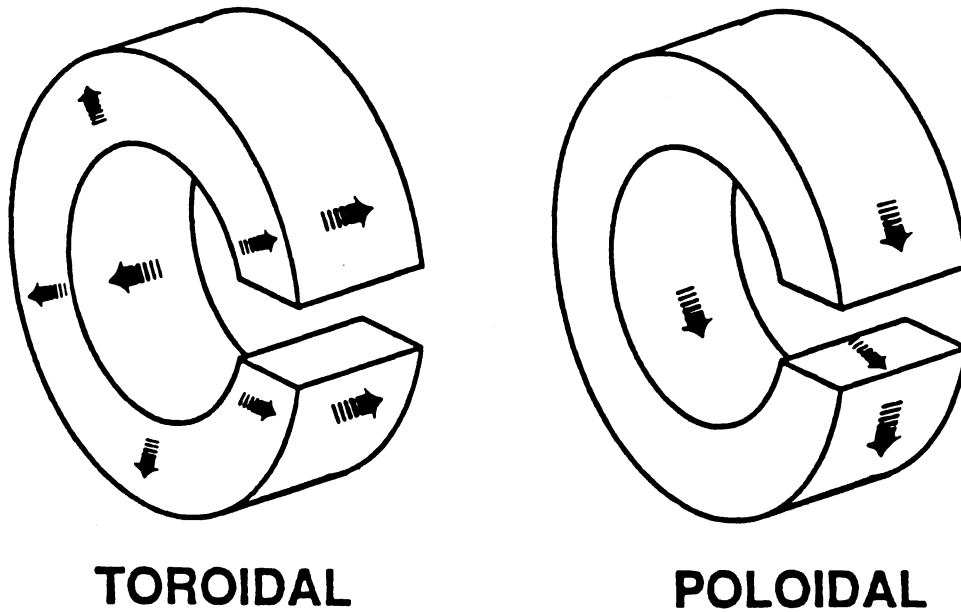


Figure 7.3-7. The current paths envisioned for the model of the passive circuit elements with resistive breaks orthogonal to the corresponding continuous current direction.

The electrical time constants of the external circuits are sufficiently short so that periodic solutions to Equations 7.3-9 and 7.3-21 are obtained simultaneously. The dissipated powers and peak reactive powers of the entire system, schematically represented in Figure 7.3-1, are derived from the calculated current and voltage waveforms.

7.4. CURRENT-DRIVE PARAMETERS

The first application of the algorithms described in Section 7.3 was to the TITAN-I design shown in Figure 7.4-1. This design has a continuous first wall, but the reflector and shield, superconducting EF coils, and the EF trim-coil circuit elements were not included in the simulations. The results of this simulation are reported in Table 7.4-I. The most prominent result of this reduced circuit simulation is that ~ 120 MW of power is dissipated in the first wall. Efforts to reduce the dissipated power initially focused on varying the toroidal-flux swing, $\delta\phi/\phi_o$, and the drive frequency, f . The results are shown in Figure 7.4-2(A). The operating window for $\delta\phi/\phi_o$ is bounded above and below for both frequencies because of a loss of field reversal. The upper bound is the result

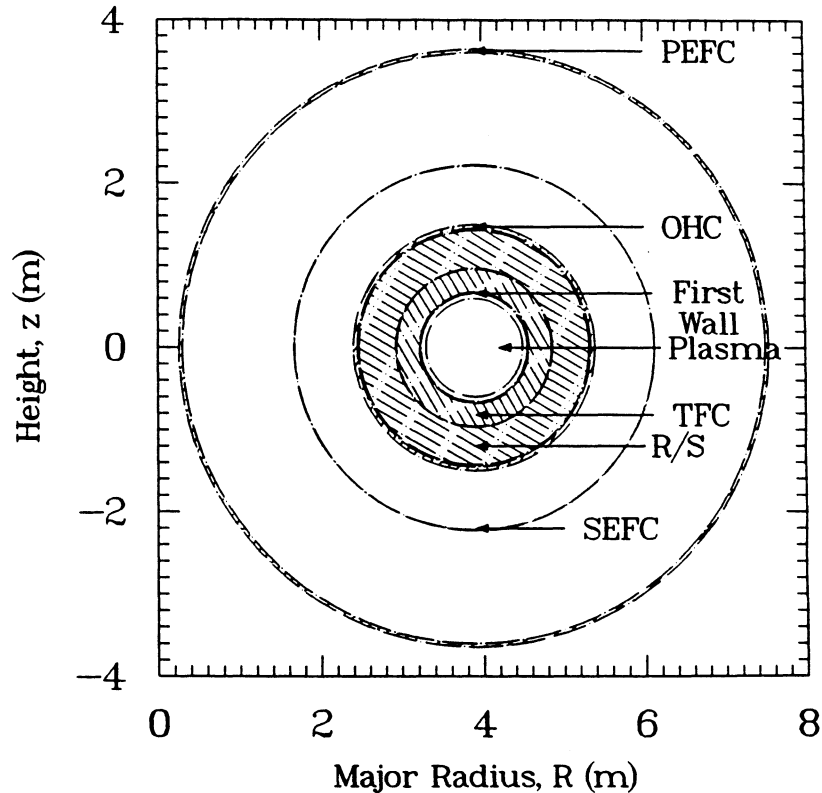


Figure 7.4-1. A cross-sectional view of the TITAN-I shell model used for OFCD calculations. The circuit elements simulated are the plasma, first wall, IBC TF coils (TFC), reflector and shield (R/S), OH coils (OHC), the trim coils (SEFC), and the superconducting EF coils (PEFC).

of too large oscillations in ϕ at a shallow reversal ($F = -0.1$). The lower bound is the result of too large oscillations in I_ϕ ($\geq 5\%$) and, hence, Θ . This lower bound causes a loss of field reversal because adherence to an F - Θ curve is strictly enforced. The $\delta\phi/\phi_o$ operating window shrinks with lower frequencies until completely disappearing at frequencies between 5 and 10 Hz. A drive frequency of 25 Hz was selected for the TITAN study because the $\delta\phi/\phi_o$ operating window is relatively unrestricted in this region, power supplies at 25 Hz are commercially available, and the effect of frequency on dissipated power has nearly saturated at 25 Hz. A flux swing of $\delta\phi/\phi_o = 0.035$ was selected because it is in the middle of the $\delta\phi/\phi_o$ operating window.

The effect of changing just the first-wall resistance at a 25-Hz drive frequency is shown in Figure 7.4-2(B). The magnetically induced voltage on the first wall, V_{FW} , is independent of the first-wall resistance, so the first-wall dissipated power scales as

Table 7.4-I.

PRELIMINARY OFCD RESULTS FOR TITAN-I DESIGN^(a)

	Without Gap	With Gap
Average plasma current, I_ϕ (MA)	17.82	17.82
Drive frequency, f (Hz)	25.	25.
Toroidal flux swing, $\delta\phi/\phi_o$	0.035	0.035
Θ variation	1.499 – 1.616	1.499 – 1.616
F variation	-0.032 – -0.173	-0.032 – -0.173
Power flow in toroidal (poloidal) circuits (MW):		
Plasma Poynting power, P_P^*	3,959.99 (247.31)	3,959.99 (247.31)
Terminal reactive power, P_H^*	325.44 (790.31)	191.20 (504.08)
Plasma dissipation, P_Ω	28.55 (0.)	28.55 (0.)
First-wall dissipation, P_{FW}	39.47 (80.73)	0.00 (0.01)
Coil dissipation, P_H	0.78 (75.77)	0.50 (47.41)
Total dissipation, P'_D	68.80 (156.5)	29.05 (47.42)
Real (lost) terminal power, P_T	42.20 (183.11)	2.44 (74.03)
Power-supply dissipated power, $P_{PS}^{(b)}$	3.25 (7.90)	1.91 (5.04)
TF-coil DC power, $P_{H,\theta}^{SS}$ (MW)	29.15	29.15
Dissipated power, P_D (MW)	236.46	83.43
Current-drive power, P_{CD} (MW)	207.31	54.28
Current-drive efficiency, I_ϕ/P_{CD} (A/W)	0.09	0.33

(a) Excluding the reflector & shield, EF coils, and trim-coils circuit elements.

(b) Assuming the power supplies are 99% efficient ($Q_{PS} = 100$).

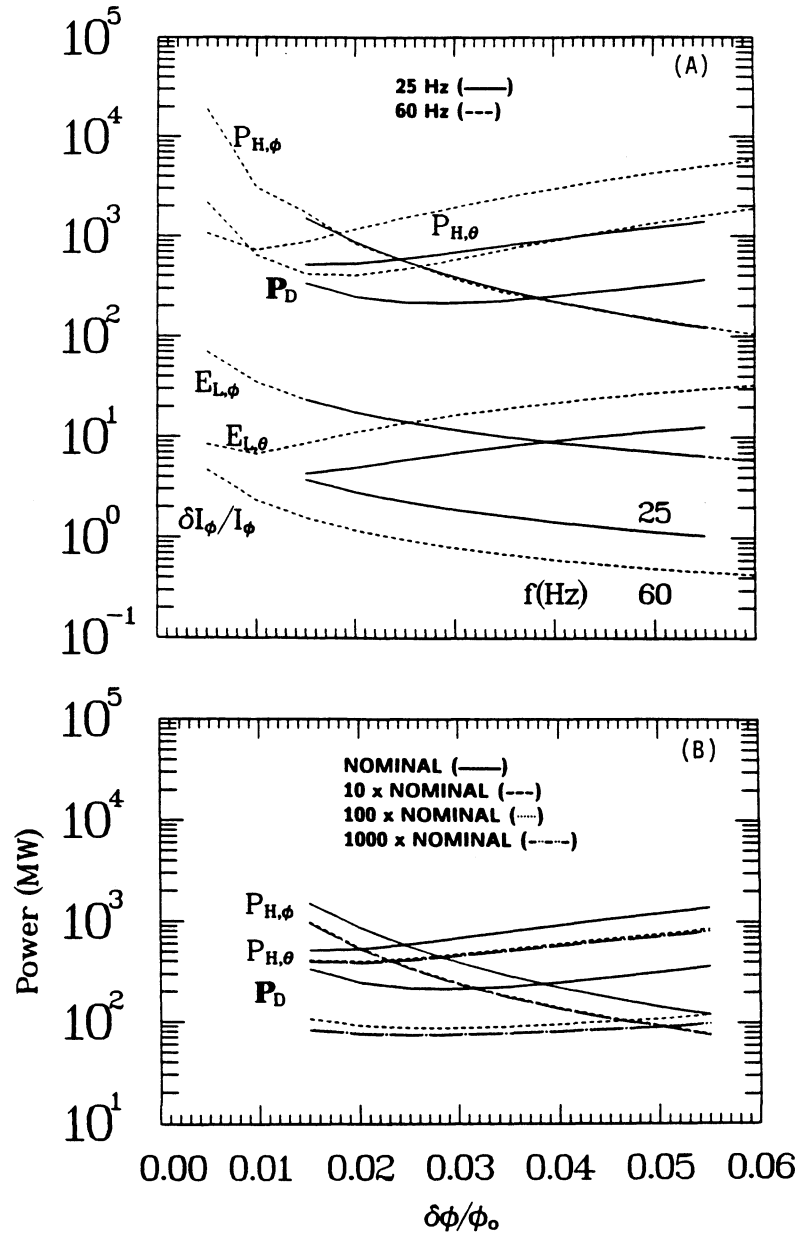


Figure 7.4-2. Power flow in TITAN-I OFCD system as a function of the amplitude of the toroidal-flux swing normalized to the mean toroidal flux (excluding the R/S, EF, and trim circuit elements). (A) Results at frequencies of 25 and 60 Hz for nominal first-wall resistance. (B) Results at 25 Hz for the nominal, 10 \times nominal, 100 \times nominal, and 1000 \times nominal first-wall resistance. Terminal reactive powers for the toroidal ($P_{H,\phi}$) and poloidal ($P_{H,\theta}$) circuits, the dissipated power (P'_D) in the plasma, first wall, TF, and OH coils, as well as electric fields at the first wall in the toroidal ($E_{L,\phi}$) and poloidal ($E_{L,\theta}$) directions and the amplitude of the plasma current oscillations normalized to the mean current ($\delta I_\phi / I_\phi$) are shown.

$P_{FW} \propto V_{FW}^2/R_{FW}$. The nominal first-wall design (and hence, resistance) is determined by thermal-hydraulics considerations (Section 10.4). To achieve the two-order-of-magnitude increase in first-wall resistance that is required to reduce the first-wall dissipated power to negligible levels, a new first-wall material that is 100 times more resistive is required. In addition, the nominal first wall provides a vertical-field penetration time of 3 ms, which falls within the 1.8-57.9-ms requirement for plasma-wall stabilization projected for TITAN (Section 5.2). This latter constraint would be difficult to meet for a much more resistive first wall. The only way to emulate an increased first-wall resistance while maintaining wall stabilization is by using gaps or insulating breaks.

The gap model described in Section 7.3 was applied to the same reduced circuit model of the TITAN-I design and is reported in Table 7.4-I in parallel with the results for a continuous first wall. The effect of the first-wall gap is primarily to reduce the dissipated power in the first wall and secondarily to reduce the coil powers. The net effect of gaps is to increase the current-drive efficiency by a factor of 3.7 over that for a continuous (without gaps) first wall.

The full capability of the circuit model was then exercised on the TITAN-I and TITAN-II designs shown in Figures 7.4-1 and 7.4-3, respectively. Initially the trim coils were disabled, which resulted in an ~ 7 -GW reactive power in the EF coils. The trim coils, subsequently, were enabled to reduce the EF-coil reactive power because the power supplies are costed at ~ 10 M\$/GW of reactive power (Section 3.3). The results of the full simulation of TITAN-I and TITAN-II for the various powers of interest as a function of $\delta\phi/\phi_o$ are shown in Figure 7.4-4. The two designs perform similarly with the exception of the TF coils. The TITAN-II TF coils are further from the plasma than in TITAN-I and, therefore, require a larger reactive power. The TF-coil dissipated power, however, is smaller in TITAN-II, even though the TITAN-I and TITAN-II DC powers are nearly equal. The TITAN-II TF coils are series wound and have a uniform current density, whereas the TITAN-I TF coils are connected in parallel with an overall radial build greater than the current-penetration skin depth with most of the current concentrating within a skin depth, as is discussed later. The gaps in both TITAN-I and TITAN-II first walls must hold off ~ 2 V in order to maintain the electrical-break effect; this condition could be met by using (1) an ~ 1 -mm wide vacuum gap or (2) even thinner amount of electrical insulator. The small-amplitude ($< 2\%$) plasma-current oscillations should not adversely affect the plasma stability or transport.

The TITAN-I and TITAN-II OFCD design points summarized in Table 7.4-II were selected from the middle of the $\delta\phi/\phi_o$ -operating window to provide a maximum safety margin against the accidental loss of field reversal. The power dissipated in the first

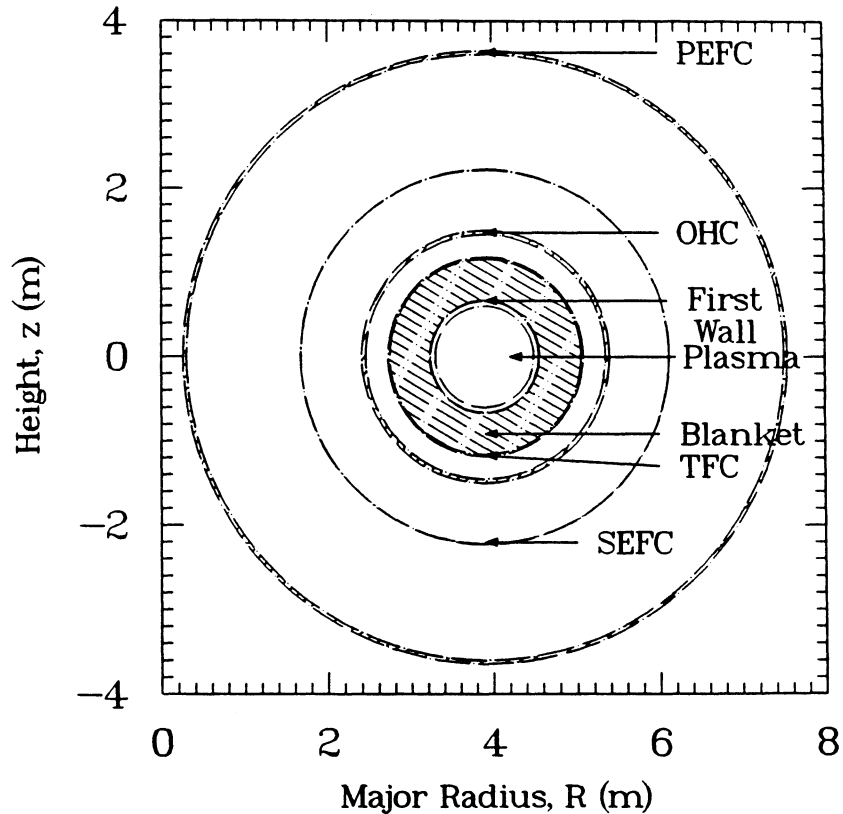


Figure 7.4-3. A cross-sectional view of the TITAN-II shell model used for OFCD calculations. The circuit elements simulated are the plasma, first wall, blanket, TF coils (TFC), OH coils (OHC), trim coils (SEFC), and superconducting EF coils (PEFC).

wall of each design (with breaks) is the same because the first walls are physically the same. The power dissipated in the TITAN-I R/S is larger than in the TITAN-II blanket primarily because of a lower R/S resistance. Because the TITAN-I R/S is positioned outside of the IBC TF coils, none of the poloidal-circuit elements couple to the R/S and no power is dissipated in the R/S from that circuit. The dissipated and reactive powers in the coils of the toroidal circuit (*i.e.*, OH, superconducting EF, and trim coils) are slightly larger for TITAN-II because the toroidal-circuit blanket inductance is larger for TITAN-II (*i.e.*, the blanket is less transparent to the power flowing through its surfaces).

The voltage waveforms for the TITAN-I and TITAN-II OFCD design points are shown in Figure 7.4-5. These waveforms indicate that the much larger TITAN-II blanket resistance causes a large (~ 100 V) induced voltage, which is not found in the TITAN-I design. The TITAN-II voltage waveforms more prominently display a phenomena com-

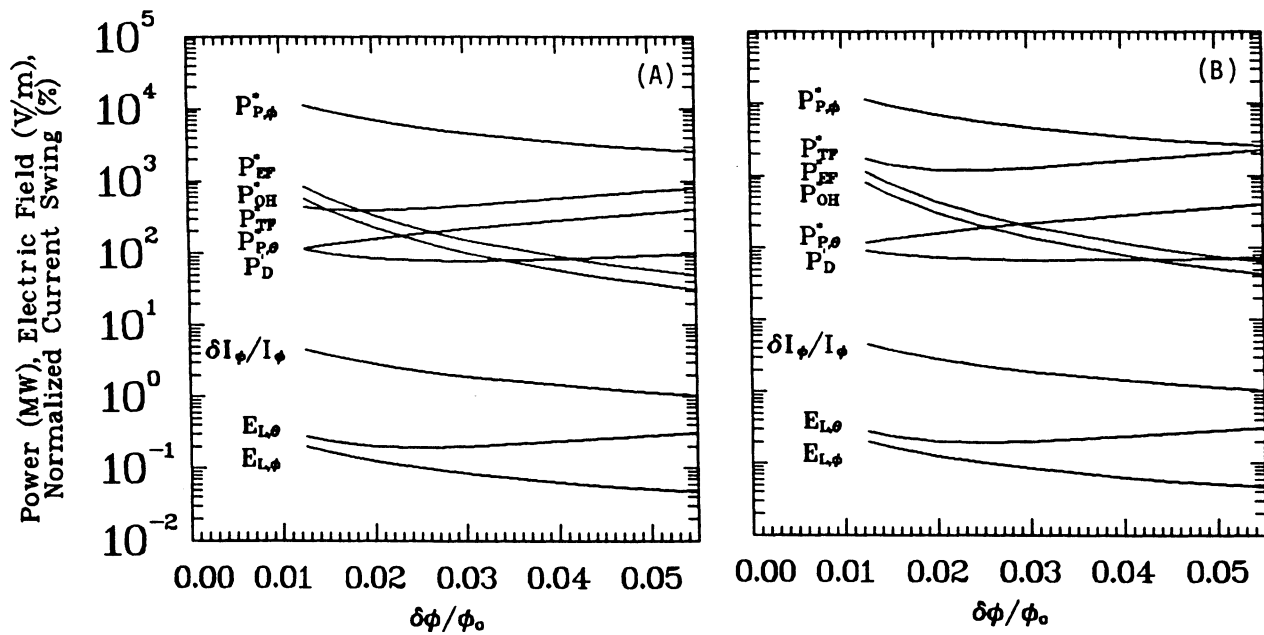


Figure 7.4-4. Power flow in TITAN-I (A) and TITAN-II (B) OFCD systems as a function of the amplitude of the toroidal-flux swing normalized to the mean toroidal flux at 25 Hz. Terminal reactive powers for the TF coils (P_{TF}^*), trim coils (P_{EF}^*), OH coils (P_{OH}^*), the plasma Poynting power in the toroidal ($P_{P,\phi}^*$) and poloidal ($P_{P,\theta}^*$) circuits, and the dissipated power (P_D^*) in the plasma, FPC components, and TF, trim, and OH coils, as well as the electric fields at the first wall in the toroidal ($E_{L,\phi}$) and poloidal ($E_{L,\theta}$) directions and the amplitude of the plasma current oscillations normalized to the mean current ($\delta I_\phi/I_\phi$).

Table 7.4-II.
COMPARISON OF OFCD IN TITAN DESIGNS

	TITAN-I	Interim TITAN-II	TITAN-II
Average plasma current, I_ϕ (MA)	17.82	17.82	17.82
Drive frequency, f (Hz)	25.	25.	25.
Toroidal-flux swing, $\delta\phi/\phi_0$	0.035	0.035	0.035
Θ variation	1.499 – 1.616	1.499 – 1.616	1.499 – 1.616
F variation	-0.032 – -0.173	-0.032 – -0.173	-0.032 – -0.173
Toroidal (poloidal) circuit power (MW):			
Plasma Poynting power, P_P^*	3959.99 (247.31)	3959.99 (247.31)	3959.99 (247.31)
Plasma dissipation, P_Ω	28.55 (0.)	28.55 (0.)	28.55 (0.)
First-wall dissipation, P_{FW}	0.00 (0.01)	0.00 (0.01)	0.00 (0.01)
Blanket dissipation, P_B	1.04 (0.)	0.01 (0.19)	0.01 (0.17)
Terminal reactive power, P_i^* (MW):			
TF coils	503.88	1413.77	1413.77
OH coils	74.92	101.99	101.99
EF coils	~ 0.	~ 0.	~ 0.
Trim coils	113.44	147.16	147.16
Coil dissipation, P_H (MW):			
TF coils	47.38	35.69	11.44
OH coils	0.13	0.17	0.17
EF coils	~ 0.	~ 0.	~ 0.
Trim coils	1.95	2.49	2.49
Real (lost) terminal power, P_T (MW):			
TF coils	74.00	62.50	38.23
OH coils	1.62	1.15	1.15
EF coils	~ 0.	~ 0.	~ 0.
Trim coils	3.44	3.46	3.46
TF-coil DC power, $P_{H,\theta}^{SS}$ (MW)	29.15	29.13	9.34
Power-supply dissipation, P_{PS} (MW) ^(a)	6.92	16.62	15.34
Total dissipation, P_D (MW)	85.93	83.74	58.19
Current-drive power, P_{CD} (MW)	56.83	54.61	48.85
Efficiency, I_ϕ/P_{CD} (A/W) ^(b)	0.33	0.33	0.36

(a) Assuming the power supplies are 99% efficient ($Q_{PS} = 100$).

(b) Based on the total power consumed including driver efficiency and transmission losses.

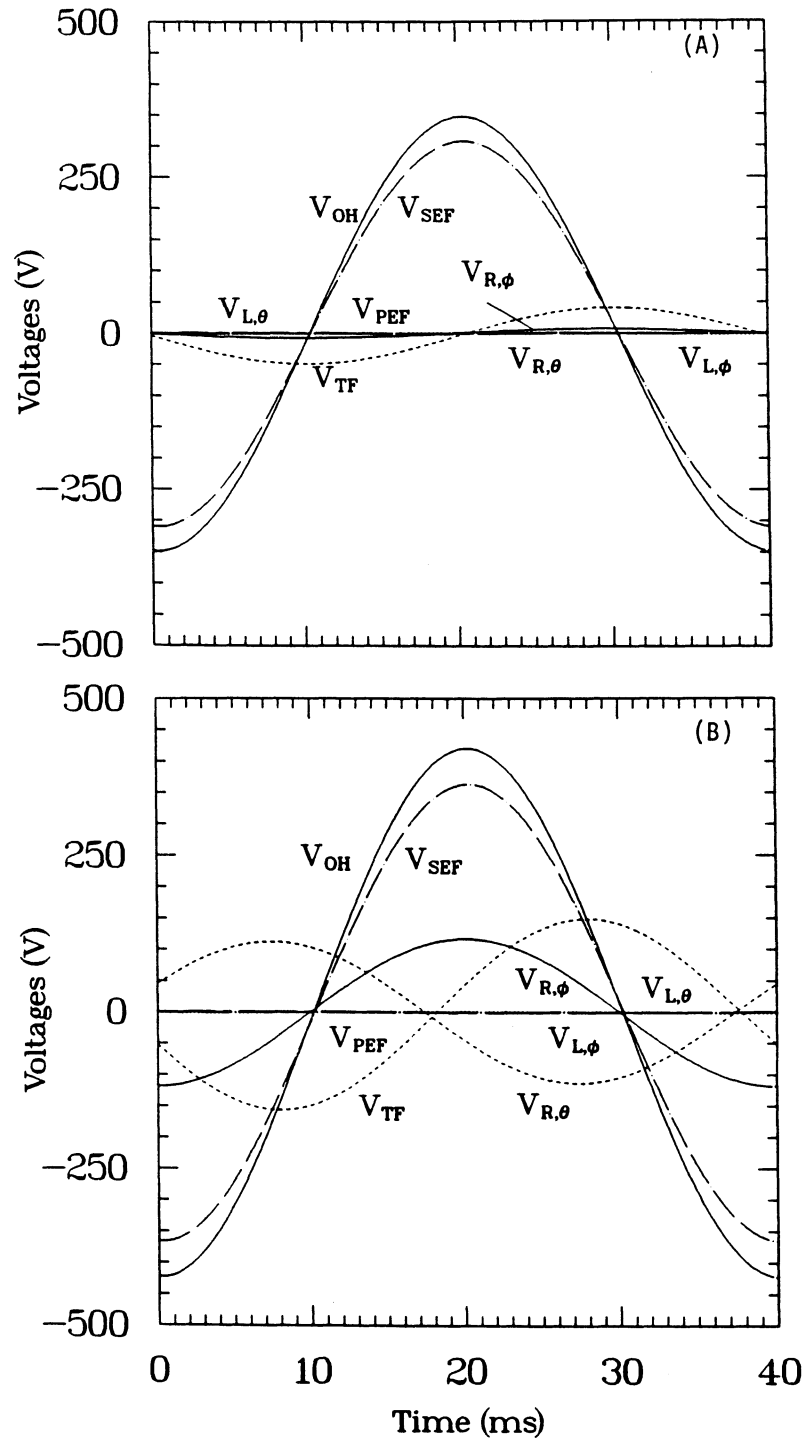


Figure 7.4-5. The voltage waveforms for TITAN-I (A) and TITAN-II (B) design for one OFCD period. The voltages across OH coils (V_{OH}), trim coils (V_{SEF}), TF coils (V_{TF}), first wall ($V_{L,\phi}$ and $V_{L,\theta}$), and across TITAN-I reflector and shield or TITAN-II blanket ($V_{R,\phi}$ and $V_{R,\theta}$) are shown.

mon to both designs: the 90° phase shift between the toroidal (V_ϕ) and poloidal (V_θ) plasma voltages, which yields the optimal current-drive efficiency, is generated by a different phase shift between the toroidal (V_{OH} and V_{SEF}) and poloidal (V_{TF}) coil voltages. The phase shift between the coil voltages is dependent upon $\delta\phi/\phi_o$ in addition to the TF-coil position.

The current waveforms for the TITAN-I and TITAN-II OFCD design points are shown in Figure 7.4-6. Even though the superconducting EF coils are maintained at a constant (albeit negligible) voltage, the current in these coils oscillates with an amplitude of ≤ 2 MA. Furthermore, the EF-coil current oscillations are out of phase with the trim- and OH-coil oscillations. The TITAN-I and TITAN-II TF-coil current waveforms are nearly the same, even though the voltage waveforms are quite different because the plasma-current and, hence, the toroidal-field waveforms are required to be identical and because the toroidal field is determined primarily by the TF coils (the toroidal field is affected only slightly by the first wall and blanket). The maximum, minimum, and average values of the voltage and current waveforms are presented in Table 7.4-III.

Whereas the TITAN-II TF-coil current density is uniform, the TITAN-I TF-coil current density has a radial variation shown in Figure 7.4-7. The expected exponential decay of the current radially through the IBC TF-coil tube bank occurs because the current-penetration skin depth is greater than the coil radial build. In addition the current from radial row to radial row incurs a phase shift. This radial non-uniformity of the IBC TF-coil current gives rise to the differences in the TITAN-I and TITAN-II TF-coil dissipated powers. The TITAN-II design ultimately dissipates less power in the first wall, blanket, and coils than TITAN-I, but has a larger terminal reactive power because of the different TF-coil designs. When the efficiency of the power supplies ($Q = 100$ assumed) is included in the current-drive efficiency, both designs operate at comparable efficiencies of ~ 0.35 A/W. This frequency is based on the total power supplied to the system, including driver efficiency and transmission losses.

7.5. SUMMARY AND CONCLUSIONS

Because of the large plasma resistance in the TITAN designs, an inductively pulsed burn would be sustained for a pulse length of the order of $L_p/R_p \simeq 200$ -400 s. Therefore, steady-state operation is essential considering issues such as the total power balance, thermal cyclic fatigue in a high-power-density environment, as well as the costs of on-site energy storage (frequent grid-assisted start-up seems unlikely) and thermal storage. An

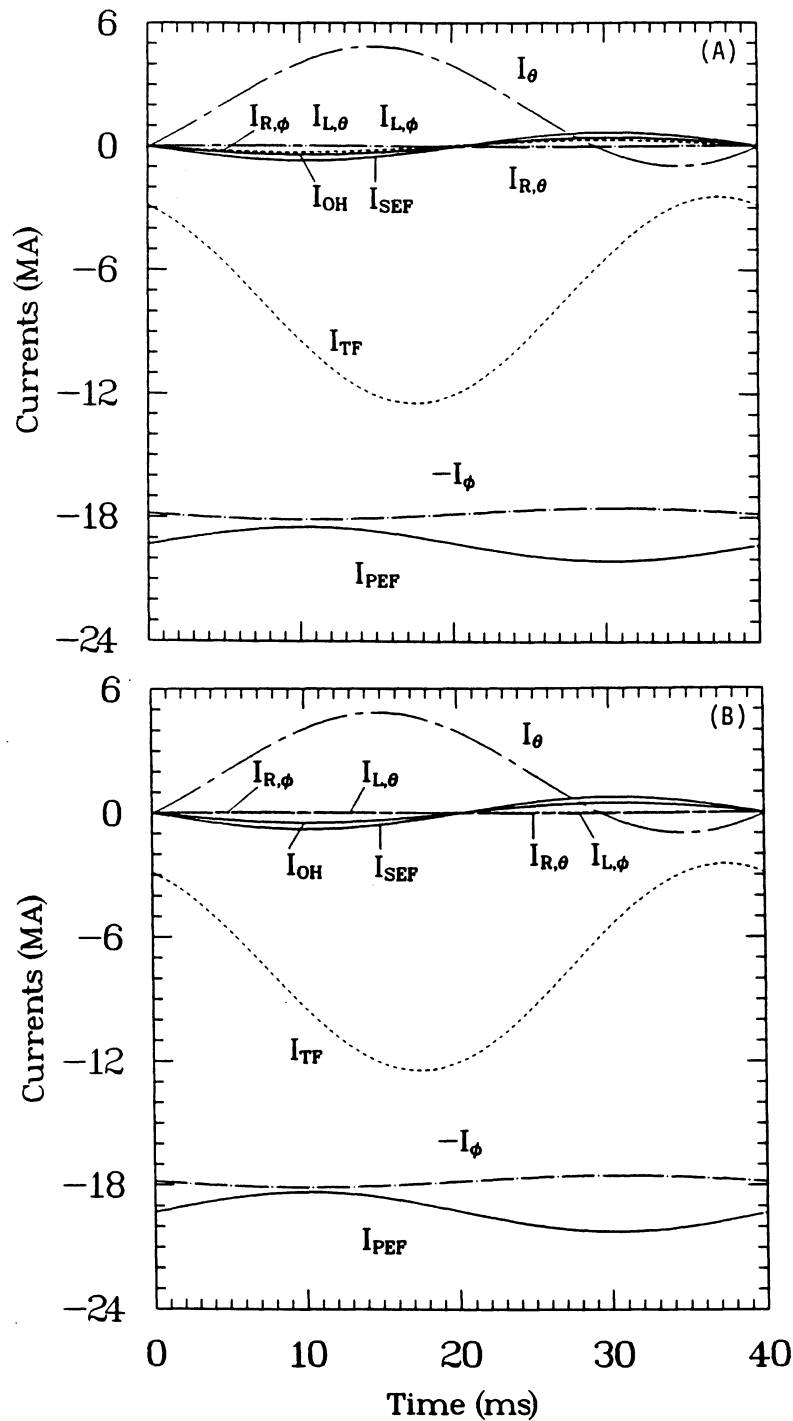


Figure 7.4-6. The current waveforms for TITAN-I (A) and TITAN-II (B) design for one OFCD period. The currents in the OH coils (I_{OH}), trim coils (I_{SEF}), superconducting EF coils (I_{PEF}), TF coils (I_{TF}), first wall ($I_{L,\phi}$ and $V_{I,\theta}$), and in TITAN-I reflector and shield or TITAN-II blanket ($I_{R,\phi}$ and $I_{R,\theta}$) are shown.

Table 7.4-III.
OFCD SINGLE-TURN VOLTAGES AND CURRENTS

	TITAN-I			TITAN-II		
	Max.	Min.	Ave. ^(a)	Max.	Min.	Ave. ^(a)
Voltage (V):						
OH coils, V_{OH}	347.	349.	0.0	420.	-423.	0.0
TF coils, V_{TF}	41.3	-49.0	-3.90	141.	-143.	-1.25
EF coils, V_{PEF}	0.0	0.0	0.0	0.0	0.0	0.0
Trim coils, V_{SEF}	308.	-310.	-0.194	363.	-366.	-0.119
First wall						
$V_{L,\theta}$	0.892	-0.898	0.0	0.892	-0.898	0.0
$V_{L,\phi}$	1.74	-1.76	0.0	1.74	-1.76	0.0
Blanket						
$V_{R,\theta}$	0.0	0.0	0.0	107.	-107.	0.0
$V_{R,\phi}$	7.23	-7.21	0.0	117.	-119.	0.0
Current (MA):						
OH coils, I_{OH}	0.411	-0.419	-0.004	0.469	-0.476	-0.004
TF coils, I_{TF}	-2.46	-12.4	-7.45	-2.46	-12.4	-7.45
EF coils, I_{PEF}	-18.5	-20.1	-19.3	-18.3	-20.2	-19.3
Trim coils, I_{SEF}	0.657	-0.701	-0.023	0.754	-0.781	-0.014
First wall						
$I_{L,\theta}$	0.032	-0.032	0.0	0.032	-0.032	0.0
$I_{L,\phi}$	0.001	-0.001	0.0	0.001	-0.001	0.0
Blanket						
$I_{R,\theta}$	0.0	0.0	0.0	0.003	-0.003	0.0
$I_{R,\phi}$	0.287	-0.286	0.0	0.0002	-0.0002	0.0
Plasma, I_ϕ	18.1	17.5	17.8	18.1	17.5	17.8

(a) Average value of x is $\langle x \rangle \equiv \tau^{-1} \int_0^\tau x(t) dt$, where τ is one OFCD period.

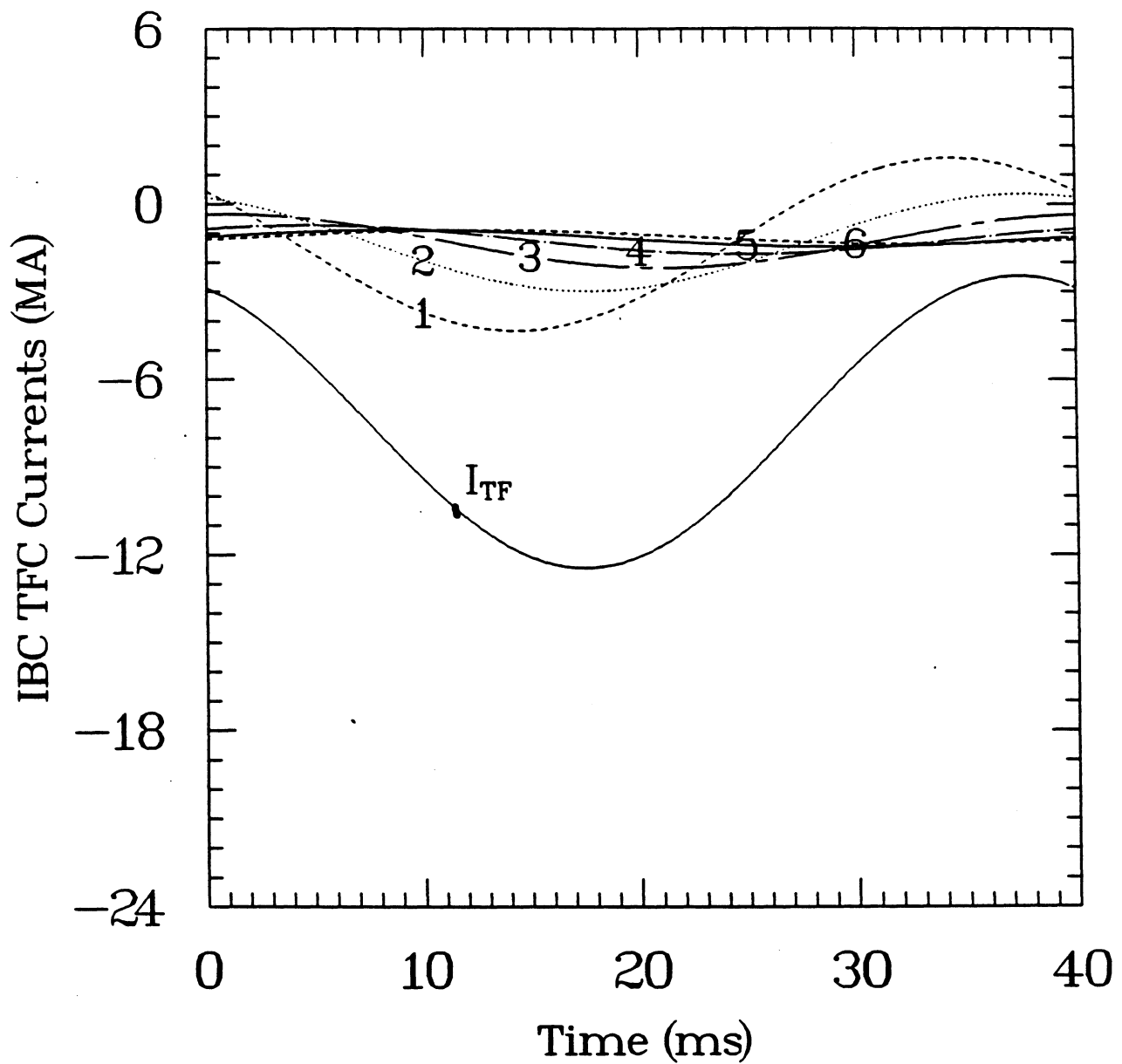


Figure 7.4-7. TITAN-I TF-coil current waveform (I_{TF}) resolved into the current waveform in each of the six radial rows of IBC tubes. Curve 1 corresponds to the inner most row of tubes, with increasing number indicating consecutively the outer rows.

inductively pulsed RFP reactor is a possibility [1]. The parameters of such a reactor, however, should be optimized to minimize the plasma resistance, which results in larger plasmas, lower power density, and possibly the use of superconducting coils throughout the FPC.

A number of current-drive options for the RFP have been considered (Section 7.2). Although the use of fast-wave current-drive schemes has not been fully explored for the RFP, the high plasma density ($n \sim 9 \times 10^{20} \text{ m}^{-3}$ in TITAN) and currents relative to those for the tokamak indicate problems with the efficiency of radio-frequency (RF) current-drive schemes. On the other hand, because of the relaxation processes in RFPs, there is no need to drive the current at the plasma center and some of the issues related to wave penetration may be negated. Bootstrap current is also expected to be low, if such current exists at all in RFPs, since β_θ and $\epsilon = r_p/R_T$ are small relative to the tokamak.

The close coupling of poloidal and toroidal currents and magnetic fields that determine the near-minimum-energy states of the RFP offers the possibility of a current-drive method based on “magnetic helicity injection” because the resistive decay of plasma current can be viewed as a dissipation of magnetic helicity [2]. For the TITAN reactors, helicity injection by the oscillating-field current drive (OFCD) has been selected as the means to sustain the toroidal plasma current.

A circuit model was developed that simulates the major elements associated with OFCD in order to determine the injected and/or dissipated powers. The model was used to quantify the need for toroidal and poloidal gaps or insulating breaks in structures such as the first wall, which will have currents induced by the OFCD. It is concluded that these breaks are needed to achieve acceptable current-drive efficiencies ($\sim 0.35 \text{ A/W}$). Detailed analysis of the TITAN-I and TITAN-II designs revealed a preference for the following: (1) series winding of all OFCD coils; (2) the positioning of these coils as close to the plasma as possible; and (3) in the case of coil sets with small amplitude oscillations about large average currents, the splitting of the coil set into a set devoted to the oscillation and another set to produce the mean current. Future work should focus on effects of field errors introduced by gaps during current oscillations, a better modeling of helicity balance and profile changes, and the generation of a better engineering understanding of the interaction of the OFCD system with other major FPC subsystems (*e.g.* equilibrium control, impurity control, and startup and shutdown systems).

REFERENCES

- [1] R. Hancox, R. A. Krakowski, and W. R. Spears, "The Reversed-Field Pinch Reactor Concept," *Nucl. Eng. and Res.* **63** (1981) 251.
- [2] M. K. Bevir and J. W. Gray, "Relaxation, Flux Consumption and Quasi Steady State Pinches," *Proc. of RFP Theory Workshop*, Los Alamos, NM (1980), Los Alamos National Laboratory report LA-8944-C (1982) 176.
- [3] D. D. Schnack, E. J. Caramana, and R. A. Nebel, "Three-Dimensional Magnetohydrodynamic Studies of the Reversed-Field Pinch," *Phys. Fluids* **28** (1985) 321.
- [4] E. J. Caramana, R. A. Nebel, and D. D. Schnack, "Nonlinear, Single-Helicity Magnetic Reconnection in the Reversed-Field Pinch," *Phys. Fluids* **26** (1983) 1305.
- [5] R. A. Scardovelli, R. A. Nebel, and K. A. Werley, "Transport Simulation of the Oscillating Field Current Drive Experiment in the ZT-40M," Los Alamos National Laboratory report LA-UR-2802.
- [6] K. F. Schoenberg, J. C. Ingraham, C. P. Munson, P. G. Weber, D. A. Baker, R. F. Gribble, *et al.*, "Oscillating-Field Current Drive Experiment in a Reversed Field Pinch," *Phys. Fluids* **31** (1988) 2285.
- [7] J. B. Taylor, "Relaxation and Magnetic Reconnection in Plasma," *Rev. Mod. Phys.* **58** (1986) 741; also "Relaxation of Toroidal Plasma and Generation of Reversed Magnetic Fields," *Phys. Rev. Lett.* **33** (1974) 1139; and "Relaxation of Toroidal Discharges," *Proc. 3rd Topical Conf. on Pulsed High-Beta Plasmas*, Abingdon (Sept. 1975), Pergamon Press, London (1976) 59.
- [8] C. W. Barnes, J. C. Fernandez, I. Henins, H. W. Hoida, T. R. Jarboe, S. O. Knox, G. J. Marklin, and K. F. McKenna, "Experimental Determination of the Conservation of Magnetic Helicity from the Balance Between Source and Spheromak," *Phys. Fluids* **29** (1986) 3415.
- [9] K. F. Schoenberg, C. J. Buchenauer, R. S. Massey, J. G. Melton, R. W. Moses, R. A. Nebel, and J. A. Phillips, " $F - \Theta$ Pumping and Field Modulation Experiments on a Reversed Field Pinch Discharge," *Phys. Fluids* **27** (1984) 548.
- [10] K. F. Schoenberg, R. F. Gribble, and D. A. Baker, "Oscillating Field Current Drive for Reversed Field Pinch Discharges," *J. Appl. Phys.* **56** (1984) 2519.

- [11] J. T. Hogan, *Bull. Am. Phys. Soc.* **31** (1986) 1548.
- [12] J. M. Finn and T. M. Antonsen, Jr., "Anomalous Current Penetration and Oscillating Current Drive in Tokamaks," *Phys. Fluids* **30** (1987) 2450.
- [13] M. Ono, G. J. Greene, D. Dajrrow, C. Forest, H. Park, and T. H. Stix, "Steady-State Tokamak Discharge via Helicity Injection," *Phys. Rev. Lett.* **59** (1987) 2165.
- [14] *Proc. Int. Workshop on Engineering Design of Next Step Reversed Field Pinch Devices*, D. B. Thomson (Ed.), Los Alamos National Laboratory (July 13-17, 1987).
- [15] R. Gross, *Fusion Energy*, Wiley and Sons, New York (1984) p. 118.
- [16] N. J. Fisch, "Theory of Current Drive in Plasmas," *Rev. Mod. Phys.* **59** (1987) 175.
- [17] M. Abdou, C. Baker, J. Brooks, D. Defreese, D. Ehst, *et al.*, "A Demonstration Tokamak Power Plant Study-Interim Report," Argonne National Laboratory report ANL/FPP/TM-154 (1982) Chapter 2.
- [18] M. Porkolab, B. Blackwell, P. Bonoli, D. Griffin, S. Knowlton, *et al.*, "Lower Hybrid Heating, Current Drive and Ion Cyclotron Heating Experiments on Alcator C and Versator II Tokamaks," *Proc. 10th Int. Conf. Plasma Phys. and Cont. Nuc. Fusion Res.*, London (September 1984) 463.
- [19] K. L. Wong and M. Ono, "Effects of Ion Cyclotron Harmonic Damping on Current Drive in the Lower Hybrid Frequency Range," *Nucl. Fusion* **24** (1984) 615.
- [20] N. J. Fisch and C. F. F. Karney, "Current Generation with Low Frequency Waves," *Phys. Fluids* **24** (1981) 27.
- [21] D. A. Ehst, "Relativistic Electron Beam Current Drive," in *FED-A, An Advanced Performance FED Based on Low Safety Factor and Current Drive*, Oak Ridge National Laboratory report ORNL/FEDC-83/1 (August 1983).
- [22] R. L. Hagenson, R. A. Krakowski, C. G. Bathke, R. L. Miller, M. J. Embrechts, *et al.*, "Compact Reversed-Field Pinch Reactors (CRFPR): Preliminary Engineering Considerations," Los Alamos National Laboratory report LA-10200-MS (1984).
- [23] S. I. Braginskii, "Transport Processes in a Plasma," in *Reviews of Plasma Physics*, M. A. Leontovich (Ed.), **1**, Consultants Bureau, New York (1965).